

Design, Synthesis, and Properties of a Six-Membered Oligofuran Macrocycle†

Anthony J. Varni,^a Manami Kawakami,^a Stephanie A. Tristram-Nagle,^b David Yaron,^a Tomasz Kowalewski,^{a*} and Kevin J. T. Noonan^{a*}

4400 Fifth Ave, Department of Chemistry, Carnegie Mellon University, Pittsburgh, Pennsylvania
15213-2617

†5000 Forbes Ave, Physics Department, Carnegie Mellon University, Pittsburgh, Pennsylvania,
15231-2617

Supporting Information

Table of Contents

Materials and Methods.....	S3-S6
Experimental Procedures for Small Molecule and Macrocycle Synthesis	S7-S13
Scheme S1. Synthesis of Bpin-FEFE-Br	S7
Synthesis of <i>hex</i>-C6FE & <i>i</i>pr-C6FE	S12-S13
DFT Optimized Structures of Furan Ester Oligomers (Figures S1-S2).....	S14
Ring Strain Calculations (Figure S3).....	S15
Synthetic Approach with M(0) vs. M(II) Catalyst (Figure S4)	S16
Transitions in UV-vis of <i>hex</i> -C6FE and Beer's Law Plot (Figures S5-6).....	S17
Repeated Cycling in CV (Figure S7).....	S18
Determination of Onset Potentials in CV Experiment (Figure S8)	S19
NMR Spectra (Figures S9-S15)	S20 - S28

HRMS Spectra (Figures S16-S19).....	S29-S30
Computational Analysis (Figures S20-S33).....	S30-S39
Comparison of HOMO and LUMO energies (Table S1).....	S31
NICS Plots for C6FE, 6FE, C6F, 6F, C5F, and C7F (Figures S20-S23).....	S32-35
ELF Plots for C6F and C6FE (Figure S24).....	S36
LOL Plots for C6F and C6FE (Figure S25).....	S36
Natural Resonance Theory Analysis (Figure S26).....	S37
¹ H NMR Aggregation Study (Figures S27-S28).....	S38-S39
¹ H NMR of <i>hex</i> -C6FE at Varying Concentrations (Figure S27).....	S38
Plot of Monomer-Dimer Fitting Model (Figure S28).....	S39
References.....	S40

Materials and Methods. All reactions and manipulations of air and water sensitive compounds were carried out under a dry N₂ atmosphere using an mBraun glovebox or standard Schlenk techniques with dried and degassed solvents. All reagents were purchased from commercial sources and used as received. Hexyl 2-bromofuran-3-carboxylate and Bpin-FE-Br were synthesized according to literature procedure.¹ (2-Dicyclohexylphosphino-2',6'-dimethoxybiphenyl) [2-(2'-amino-1,1'-biphenyl)]palladium(II) methanesulfonate or SPhos-Pd-G3 and 2,2,6,6-tetramethylpiperidinylmagnesium chloride lithium chloride complex in THF/Toluene (TMPMgCl·LiCl) are available from Sigma-Aldrich.

All solvents and chemicals used for extraction and column chromatography were used as received. Flash chromatography was completed using a Biotage Isolera One Flash Chromatography System using Aldrich technical grade silica gel (pore size 60 Å, 70-230 mesh, 63-200 µm).

NMR Analysis. All NMR experiments were collected at 300 K on a two-channel Bruker Avance III NMR instrument equipped with a Broad Band Inverse (BBI) probe, operating at 500 MHz for ¹H (126 MHz for ¹³C, 160 MHz for ¹¹B). The ¹H NMR spectra are referenced to CHCl₃ (7.26 ppm) and the ¹³C NMR spectra are referenced to CDCl₃ (77.2 ppm). ¹¹B spectra were referenced to the lock signal. In the ¹³C NMR spectra collected for borylated arenes, no signal is observed for the carbon atom directly attached to the boron due to quadrupolar relaxation.

Mass Spectrometry. DART-MS (positive mode, 150-250 °C) and ESI-MS measurements were performed on a Thermo Scientific Exactive Plus EMR Orbitrap Mass Spectrometer with He as the carrier gas. Samples were prepared as 0.2 mg/mL solutions (in diethyl ether or methanol). In some cases, [2M + H]⁺ and [M + NH₄]⁺ species were also observed.

Raman Spectroscopy. Optical microscope images and Raman spectra of thin films (drop-cast onto pre-cleaned silicon wafers from 1-5 mg/mL solutions in CHCl_3) were recorded using a Horiba XplorRA ONE with a 532 nm laser.

Infrared Spectroscopy. FTIR attenuated total reflectance spectroscopy was performed using a PerkinElmer Frontier FTIR spectrometer with a germanium crystal. Spectra were acquired with a 0.25 cm^{-1} resolution over a range of $700\text{-}4000 \text{ cm}^{-1}$. Using the PerkinElmer software, the spectra were corrected for attenuated total reflectance mode.

Cyclic Voltammetry. Electrochemical potentials were determined using a Bio-Logic SP-150 potentiostat with a potential sweep rate of 35 mV/s . A 1 mm^2 glassy carbon working electrode, a platinum coil counter electrode, and a silver wire pseudo-reference electrode were employed for the measurements. The voltammogram was referenced using Fc/Fc^+ as an internal standard [0.46 V ($E_{\text{Fc}/\text{Fc}^+}$) vs. SCE].² Tetra-*n*-butylammonium hexafluorophosphate was used as the supporting electrolyte at a concentration of 0.1 M in CH_2Cl_2 . The CH_2Cl_2 solutions with the supporting electrolyte and analyte were degassed for 10 min with Ar prior to measurement.

UV-Vis Spectroscopy. UV-Vis spectra of all polymers were recorded on a Varian Cary 5000 spectrophotometer. Prior to recording the spectra for all polymers, a 100% transmittance sample was taken of the cuvette (quartz, $10 \text{ mm} \times 10 \text{ mm}$). The “blank” of the solvent (CHCl_3) was then collected for baseline subtraction during analysis.

Powder X-ray Diffraction. Powder X-ray diffraction data were collected using a Rigaku rotating anode RUH3R. Samples were prepared by loading powder into the tip of 1 mm quartz capillaries. These capillaries were then loaded into a custom holder such that the sample was in line with the beam. Cu $K\alpha$ radiation with $\lambda = 1.5418 \text{ \AA}$ was used; beam size was $0.5 \times 0.5 \text{ mm}$, focused with a Xenocs Fox2D focusing collimator. 2D images were collected on a Rigaku Mercury CCD detector

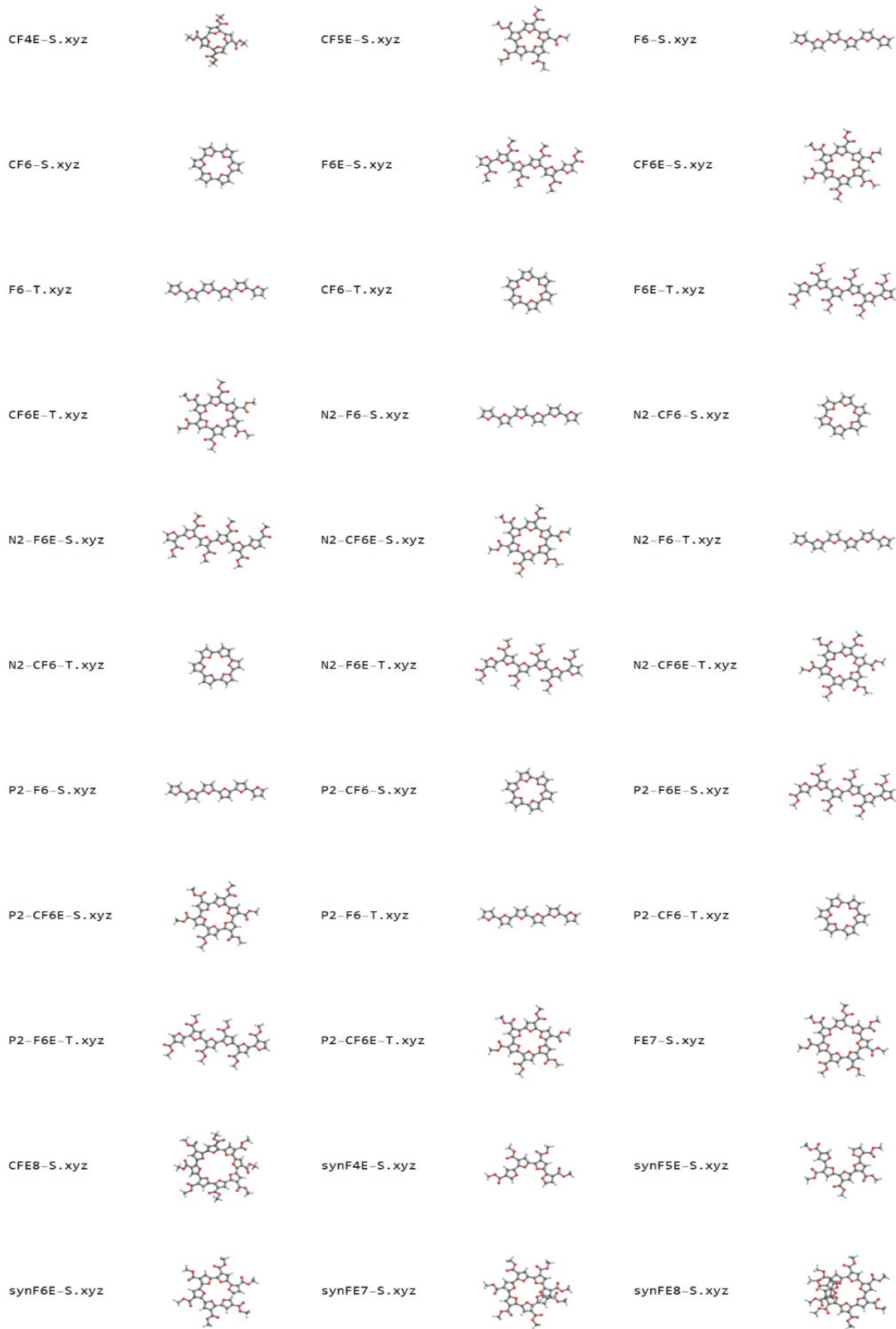
in 1 min dezingered scans. The sample-to-CCD distance was 71.3 mm, calibrated with silver behenate powder ($d = 58.367 \text{ \AA}$).

Computational Studies. Density functional theory (DFT), time-dependent DFT (TD-DFT), and nucleus-independent chemical shift (NICS) calculations were performed with Gaussian 09 and Gaussian 16.³ Geometry optimizations for all compounds were performed at the B3LYP-D3/6-31G (d,p) level. TD-DFT calculations were performed at the CAM-B3LYP 6-31G (d,p) level using the Polarizable Continuum Model (PCM) using the integral equation formalism variant (IEFPCM) and CH_2Cl_2 or CHCl_3 as the solvent. Natural Bond Orbital and Natural Resonance Theory calculations were performed using the NBO 7 package.⁴ Natural transition orbital (NTO), localized-orbital locator (LOL^{5,6}), and electron localization function (ELF⁷) analyses were carried out using the Multiwfn package^{8,9} with results from DFT (NBO, LOL, ELF) or TD-DFT (NTO) calculations. Isosurface images were generated in Multiwfn or using custom routines written in Mathematica (Wolfram Research, Inc).

NICS calculations were performed using the Gauge-Independent Atomic Orbital (NMR-GIAO) method at the B3LYP/6-31G(d,p) level on a polar grid of points placed 1 angstrom above the plane of the macrocycle. The results were visualized using Mathematica with custom written routines.

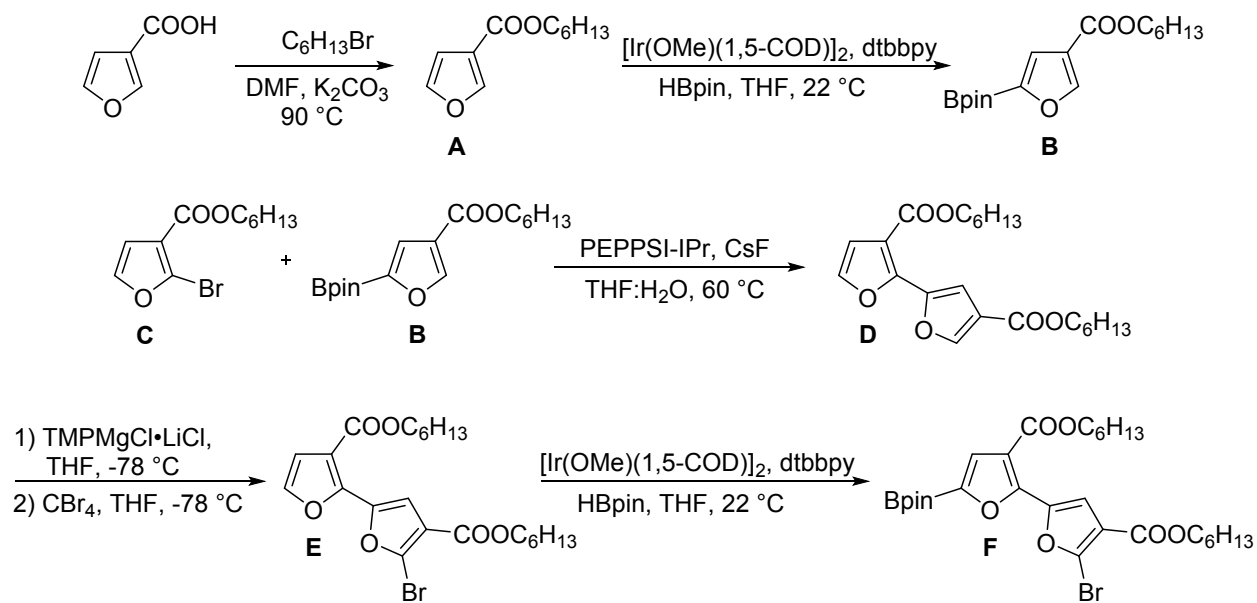
Optimized geometries for all relevant structures are included as a compressed folder with relevant .xyz files. The key is illustrated on the following page, with the corresponding labels that follow the form: (q)-(C)#F(E)-S/T, where # corresponds to the number of repeat units, and optional characters shown in parentheses indicate the molecule form (C – cyclic, no label - linear), the side group (E – methyl ester, no label – unsubstituted), charges (q=N2 for dianion and P2 for dication, no label – neutral) and S or T refers to singlet or triplet state.

File Names For .xyz coordinate files



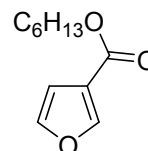
Experimental Procedures

Scheme S1. Synthesis of “dimer-type” monomer Bpin-FEFE-Br.



Compound A. Hexyl furan-3-carboxylate.

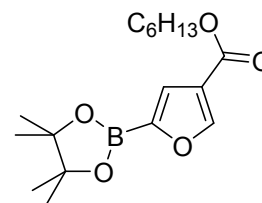
An oven-dried 250 mL Schlenk flask was charged with furan-3-carboxylic acid (15.29 g, 136.5 mmol), K_2CO_3 (56.40 g, 408.1 mmol) and 250 mL of dimethylformamide and sealed with a septum. The flask was immersed in an oil bath at $90\text{ }^\circ\text{C}$, put under a positive flow of N_2 and stirred for 2 h. 1-Bromohexane (33.68 g, 204.0 mmol) was subsequently added via a syringe, and the reaction was stirred for 18 h. The reaction mixture was cooled to room temperature, diluted with 600 mL of water and transferred to a separatory funnel. The aqueous layer was extracted with diethyl ether ($3 \times 150\text{ mL}$), and the combined organic extracts were washed with water and brine. The solution was dried using Na_2SO_4 and concentrated using rotary evaporation. The crude product was purified by vacuum distillation at 175 mtorr. The oil bath used to heat the apparatus was set to $75\text{ }^\circ\text{C}$. The final product was collected as a clear, colorless oil (23.47 g, 88%).



^1H NMR (500 MHz, CDCl_3) δ 8.00 (dd, $J = 1.6, 0.7$ Hz, 1H), 7.42 (t, $J = 1.8$ Hz, 1H), 6.74 (dd, $J = 2.0, 0.7$ Hz, 1H), 4.24 (t, $J = 6.7$ Hz, 2H), 1.75 – 1.66 (m, 2H), 1.45 – 1.27 (m, 6H), 0.94 – 0.86 (m, 3H).

^{13}C NMR (126 MHz, CDCl_3) δ 163.4, 147.7, 143.8, 119.8, 110.0, 64.8, 31.6, 28.8, 25.8, 22.7, 14.2.

Compound B. Hexyl 5-(4,4,5,5-tetramethyl-1,3,2-dioxaborolan-2-yl)furan-3-carboxylate.



In a N_2 filled glovebox, a 150 mL round-bottomed flask was charged with 4,4'-di-*tert*-butyl-2,2'-dipyridyl (dtbbpy) (0.21 g, 0.78 mmol), (1,5-cyclooctadiene)(methoxy)iridium(I) dimer (0.25 g, 0.38 mmol) and 15 mL of THF, and stirred for 30 min. To this mixture, pinacolborane (HBpin) (9.12 g, 71.3 mmol) was added dropwise along with 15 mL THF, and the mixture was stirred for an additional 30 min. The color of the reaction went from light green-brown to dark red-brown during that period. The reaction mixture was diluted with an additional 60 mL THF, and compound A (14.7 g, 75.0 mmol), dissolved in 15 mL of THF, was added to the reaction mixture dropwise (H_2 gas evolves in this step). An additional 15 mL THF was used to aid quantitative transfer of compound A to the reaction flask, bringing the total amount of THF to 120 mL. The solution was kept in the glovebox and stirred overnight. The crude mixture was then removed from the glovebox, concentrated, and purified by vacuum distillation at 170 mtorr. The sand used to heat the apparatus was set to 170 $^\circ\text{C}$. The final product was collected as a clear, colorless oil (17.58 g, 73%).

^1H NMR (500 MHz, CDCl_3) δ 8.17 (d, $J = 0.6$ Hz, 1H), 7.36 (d, $J = 0.6$ Hz, 1H), 4.22 (t, $J = 6.7$ Hz, 2H), 1.74 – 1.64 (m, 2H), 1.44 – 1.26 (m, 18H), 0.94 – 0.84 (m, 3H).

^{13}C NMR (126 MHz, CDCl_3) δ 163.1, 152.0, 123.0, 120.5, 84.8, 64.9, 31.6, 28.8, 25.8, 24.9, 22.7, 14.2.

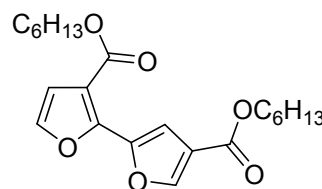
^{11}B NMR (160 MHz, CDCl_3) δ 27.2.

HR-EIMS (m/z): $[\text{M}+\text{H}]^+$ calculated for $\text{C}_{17}\text{H}_{28}\text{BO}_5$, 323.2030; found, 323.2020.

Compound C. Hexyl 2-bromofuran-3-carboxylate.

See reference 1 for ^1H & ^{13}C NMR spectra.

Compound D. Dihexyl [2,2'-bifuran]-3,4'-dicarboxylate.



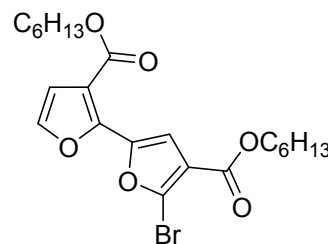
In a N_2 filled glovebox, an oven-dried 250 mL Schlenk flask was charged with PEPPSI-IPr (0.26 g, 0.38 mmol), CsF (4.00 g, 26.3 mmol), compound **B** (5.10 g, 15.83 mmol), and compound **C** (3.70 g, 13.50 mmol). 130 mL additional THF was added to the flask, which was then sealed, removed from the glovebox, and opened to N_2 on a Schlenk manifold. The flask was then placed in a $60\text{ }^\circ\text{C}$ oil bath and 4.3 mL of degassed H_2O was added with a syringe. The reaction was stirred overnight, after which the flask was cooled to room temperature. The crude mixture was concentrated via rotary evaporation and transferred to a separatory funnel. 500 mL of H_2O was added, and the aqueous layer was extracted with diethyl ether ($3 \times 150\text{ mL}$). The combined organic extracts were washed with water and brine, dried using Na_2SO_4 , and concentrated using rotary evaporation. The crude product was purified by column chromatography (gradient from 1:0 to 1:3 hexanes: CH_2Cl_2). The final product was collected as a viscous, slightly yellow oil (4.74 g, 90%).

^1H NMR (500 MHz, CDCl_3) δ 8.08 (d, $J = 0.7\text{ Hz}$, 1H), 7.74 (d, $J = 0.7\text{ Hz}$, 1H), 7.42 (d, $J = 2.0\text{ Hz}$, 1H), 6.82 (d, $J = 2.0\text{ Hz}$, 1H), 4.28 (t, $J = 6.7\text{ Hz}$, 2H), 4.26 (t, $J = 6.7\text{ Hz}$, 2H), 1.80 – 1.68 (m, 4H), 1.47 – 1.27 (m, 12H), 0.95 – 0.84 (m, 6H).

^{13}C NMR (126 MHz, CDCl_3) δ 162.9, 162.8, 147.9, 147.7, 145.6, 141.9, 121.7, 114.4, 112.7, 112.4, 65.2, 65.1, 31.62, 31.61, 28.83, 28.79, 25.83, 25.79, 22.7, 14.2. Though 12 carbon signals are expected for the two C_6H_{13} groups, the CH_3CH_2 at the end of each chain are overlapping and only 10 total aliphatic signals are observed.

HR-EIMS (m/z): $[\text{M}+\text{H}]^+$ calculated for $\text{C}_{22}\text{H}_{31}\text{O}_6$, 391.2121; found, 391.2111.

Compound E. Dihexyl 5'-bromo-[2,2'-bifuran]-3,4'-dicarboxylate.



An oven-dried 250 mL Schlenk flask was charged with compound **D** (5.09 g, 13.0 mmol) and vacuum backfilled 3 times. 130 mL of dry

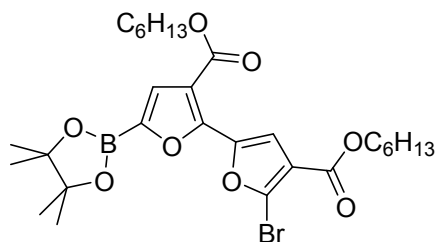
THF was added, and the solution was cooled to $-78\text{ }^\circ\text{C}$ using a dry-ice acetone bath. Then, a 1 M solution of 2,2,6,6-tetramethylpiperidylmagnesium chloride lithium chloride complex ($\text{TMPMgCl}\cdot\text{LiCl}$) in THF/toluene (15.4 mL, 15.4 mmol) was added to the solution by syringe over a 10 min period. The reaction mixture was stirred for 5.5 h at $-78\text{ }^\circ\text{C}$, then CBr_4 (7.20 g, 21.7 mmol) in 20 mL dry THF was added dropwise with a syringe over 25 min. The reaction mixture was stirred overnight and slowly warmed to room temperature. 1 M HCl solution (10 mL) was added to quench the reaction mixture. The reaction mixture was then concentrated by rotary evaporation. The remaining solution was transferred to a separatory funnel, diluted with 500 mL of DI H_2O and extracted with diethyl ether ($3 \times 150\text{ mL}$). The combined organic extracts were washed with water and brine, dried using Na_2SO_4 , and concentrated using rotary evaporation. The crude product was purified by column chromatography (gradient from 1:0 to 1:3 hexanes: CH_2Cl_2). The final product was collected as an off white solid (3.96 g, 65%).

^1H NMR (500 MHz, CDCl_3) δ 7.76 (s, 1H), 7.44 (d, $J = 1.9$ Hz, 1H), 6.82 (d, $J = 1.9$ Hz, 1H), 4.29 (t, $J = 6.8$ Hz, 2H), 4.28 (t, $J = 6.8$ Hz, 2H) 1.81 – 1.69 (m, 4H), 1.48 – 1.28 (m, 12H), 0.96 – 0.84 (m, 6H).

^{13}C NMR (126 MHz, CDCl_3) δ 162.7, 161.8, 146.8, 146.3, 142.2, 129.8, 119.7, 114.7, 114.6, 112.7, 65.4, 65.3, 31.61, 31.60, 28.78, 28.76, 25.84, 25.80, 22.7, 14.19, 14.18. Though 12 carbon signals are expected for the two C_6H_{13} groups, one of the methylene signals is overlapping and only 11 total aliphatic signals are observed.

HR-EIMS (m/z): $[\text{M}+\text{H}]^+$ calculated for $\text{C}_{22}\text{H}_{30}\text{BrO}_6$, 469.1226; found, 469.1224.

Compound F. Dihexyl 5'-bromo-5-(4,4,5,5-tetramethyl-1,3,2-dioxaborolan-2-yl)-[2,2'-bifuran]-3,4'-dicarboxylate.



In a N_2 filled glovebox, a 20 mL scintillation vial was charged with 4,4'-di-*tert*-butyl-2,2'-dipyridyl (dtbbpy) (0.023 g, 0.086 mmol), (1,5-cyclooctadiene)(methoxy)iridium(I) dimer (0.028 g, 0.042 mmol) and 1 mL of THF, and stirred for 45 min. To this mixture, pinacolborane (HBpin) (0.255 g, 1.99 mmol) was added dropwise and the mixture was stirred for an additional 45 min. The color of the reaction went from light green-brown to dark red-brown during that period. Compound **E** (0.78 g, 1.67 mmol) was then dissolved in 4 mL of THF and added to the reaction mixture dropwise (H_2 gas evolves in this step). The solution was kept in the glovebox and stirred for 24 h. The crude mixture was then removed from the glovebox, concentrated, and purified by column chromatography (gradient from 100% hexanes to 100% CH_2Cl_2). The final product was collected as a white crystalline solid (0.742 g, 75%).

^1H NMR (500 MHz, CDCl_3) 7.86 (s, 1H), 7.45 (s, 1H), 4.28 (t, $J = 6.8$ Hz, 2H), 4.26 (t, $J = 6.8$ Hz, 2H), 1.80 – 1.68 (m, 4H), 1.47 – 1.27 (m, 24H), 0.95 – 0.84 (m, 6H).

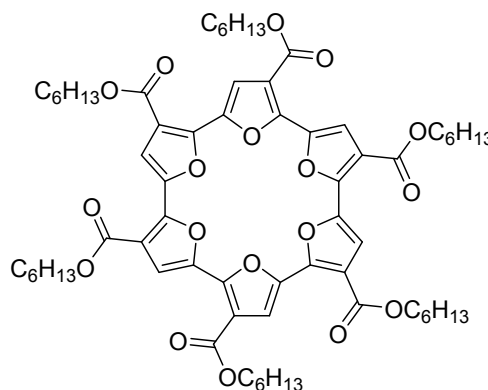
^{13}C NMR (126 MHz, CDCl_3) δ 162.6, 161.8, 150.4, 146.2, 130.4, 125.8, 119.7, 115.8, 115.1, 85.0, 65.4, 65.2, 31.7, 31.6, 28.80, 28.76, 25.9, 25.8, 24.9, 22.74, 22.73, 14.22, 14.20.

^{11}B NMR (160 MHz, CDCl_3) δ 27.0.

HR-EIMS (m/z): $[\text{M}+\text{H}]^+$ calculated for $\text{C}_{28}\text{H}_{41}\text{BBrO}_8$, 595.2078; found, 595.2054.

Compound G. Hexyl-ester macrocycle (*hex-C6FE*).

In a N_2 filled glovebox, a 100 mL Schlenk flask was charged with Compound F (0.100 g, 0.168 mmol), $\text{K}_3\text{PO}_4\cdot\text{H}_2\text{O}$ (78 mg, 0.336 mmol), and SPhos-Pd-G3 (0.010 g, 0.013 mmol). 84 mL of dry THF was added, and the flask was removed from the glovebox and opened to



N_2 on a Schlenk manifold. The flask was lowered into an oil bath at 50 °C and stirred for 1 min before degassed H_2O (2.81 mL) was added. The reaction mixture was stirred for 5 h, after which the flask was raised from the oil bath and cooled to room temperature. The reaction mixture was then concentrated by rotary evaporation, and methanol was added to precipitate the macrocycle and polymer products. After sonication for 6 min, the crude product was isolated from residual small molecule byproducts with vacuum filtration. The crude product was then purified by column chromatography (gradient from 100% hexanes to 100% CH_2Cl_2). The final product was collected as a red solid (0.022 g, 34%).

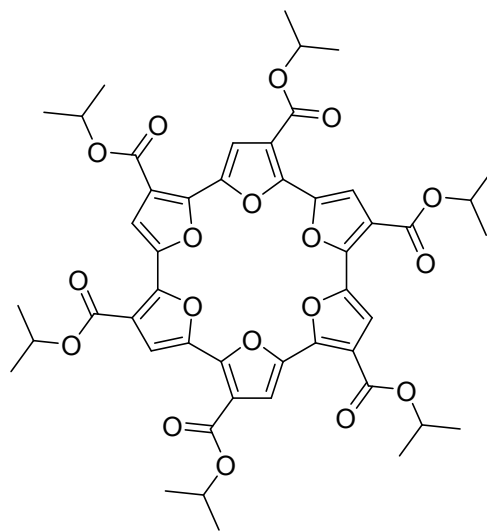
^1H NMR (500 MHz, CDCl_3) δ 7.50 (s, 6H), 4.19 (t, $J = 7.2$ Hz, 12H), 1.79 – 1.67 (m, 12H), 1.44 – 1.29 (m, 36H), 0.95 – 0.86 (m, 18H).

^{13}C NMR (126 MHz, CDCl_3) δ 162.0, 149.1, 144.2, 116.4, 116.3, 65.2, 31.7, 28.8, 25.7, 22.8, 14.2.

MALDI-TOF MS (m/z): $[\text{M}]^+$ calculated for $\text{C}_{66}\text{H}_{84}\text{O}_{18}$, 1164.5658; found, 1164.73.

Compound H. Isopropyl-ester macrocycle (*i*pr-C6FE).

In a N₂ filled glovebox, a 20 mL scintillation vial was charged with Compound G (0.018 g, 0.015 mmol) and sodium isopropoxide (32 mg, 0.39 mmol). 4 mL dry THF and 1.5 mL dry isopropanol were added, and the reaction stirred for 16 h. The reaction mixture was removed from the glovebox and quickly poured into 100 mL of



deionized H₂O. The aqueous layer was extracted with CHCl₃ (3 × 30 mL). The combined organic extracts were concentrated using rotary evaporation, and the crude product was then purified by column chromatography eluting with CHCl₃. The final product was collected as a red solid (13 mg, 95%).

¹H NMR (500 MHz, CDCl₃) δ 7.55 (s, 6H), 5.20 (septet, *J* = 6.3 Hz, 6H), 1.37 (d, *J* = 6.4 Hz, 36H).

¹³C NMR (126 MHz, CDCl₃) δ 161.6, 148.8, 144.2, 116.9, 116.6, 68.8, 22.2.

MALDI-TOF MS (*m/z*): [M]⁺ calculated for C₁₂H₁₇BBrO₂, 912.2841; found, 914.131.

DFT Optimized Structures of Furan Ester Oligomers

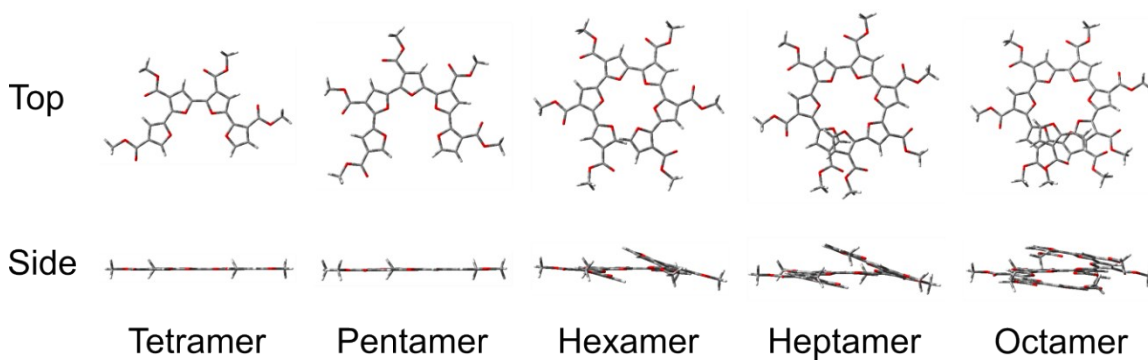


Figure S1. Optimized structures of uncyclized furan ester oligomers using DFT at the B3LYP-D3 6-31G(d,p) level.

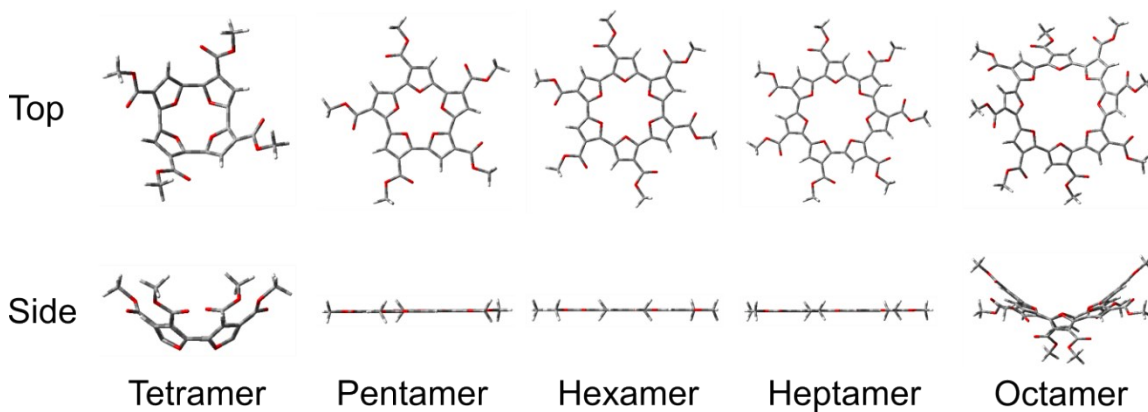


Figure S2. Optimized structures of cyclized furan ester oligomers using DFT at the B3LYP-D3 6-31G(d,p) level.

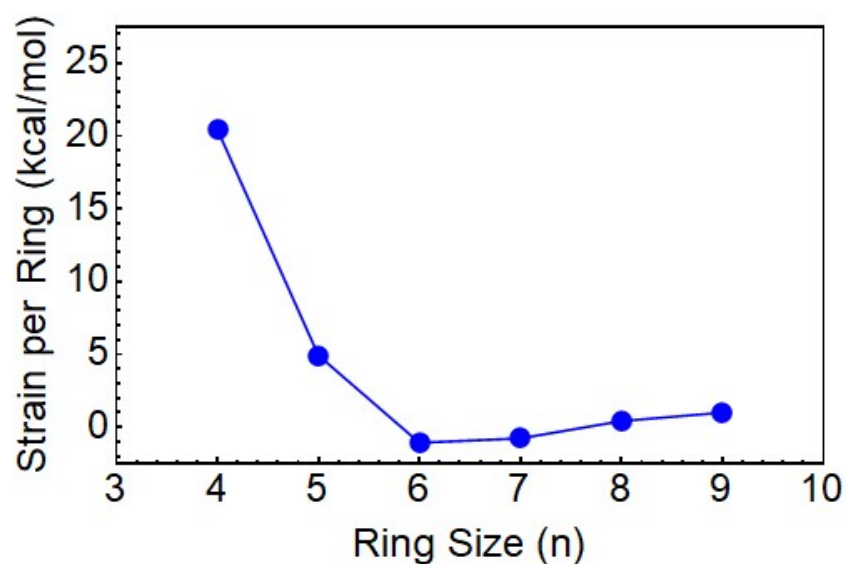


Figure S3. Ring strain for C4-9FE. These values were calculated with Equation 1, which was adapted from a previous report.¹⁰

(Equation 1)

$$\text{Strain per Ring} = \frac{(E_{\text{calc}} - n E_{\text{mon}})}{n}$$

n = number of repeat units

E_{calc} = total electronic energy value for optimized CnFE oligomer

$$E_{\text{mon}} = (E_{18\text{FE}} - E_{6\text{FE}})/12$$

E_{mon} is the total energy of a single repeat unit/monomer without end groups. This was determined by looking at the energy difference of an 18-mer and 6-mer

$E_{18\text{FE}}$ = electronic energy value for optimized 18FE oligomer (*anti* form)

$E_{6\text{FE}}$ = electronic energy value for optimized 6FE oligomer (*anti* form)

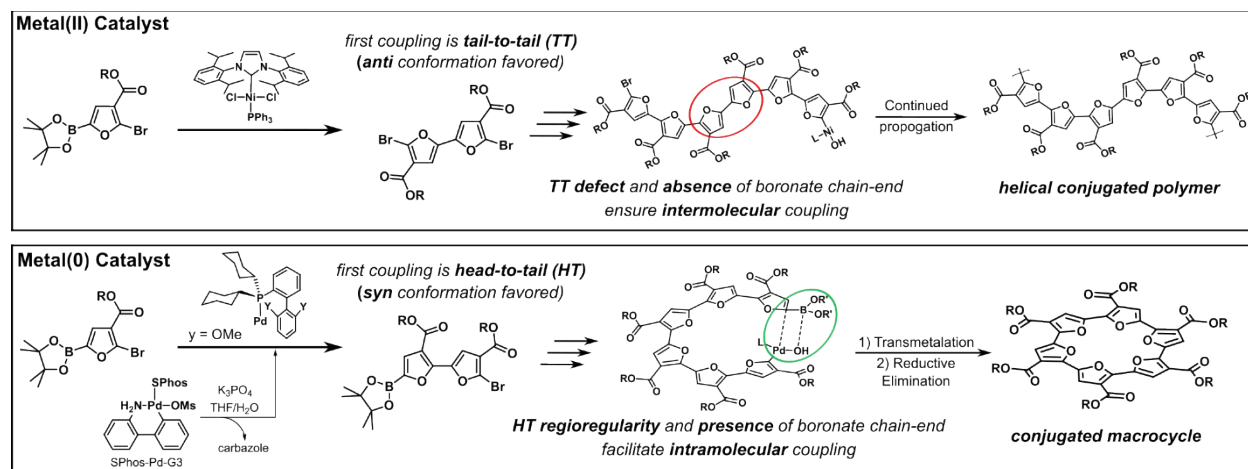


Figure S4. Comparison of oligomer growth with a metal(II) catalyst and metal(0) catalyst. With a metal(II) catalyst, the first cross-coupling results in a tail-to-tail (TT) defect, which prevents cyclization due to both oligomer geometry and chain-end functionalities (both C-X bonds). With a metal(0) catalyst, the first cross-coupling is head-to-tail, and ultimately cyclization is facilitated by the oligomer's preference for *syn* conformation as well as complementary chain-end functionalities.

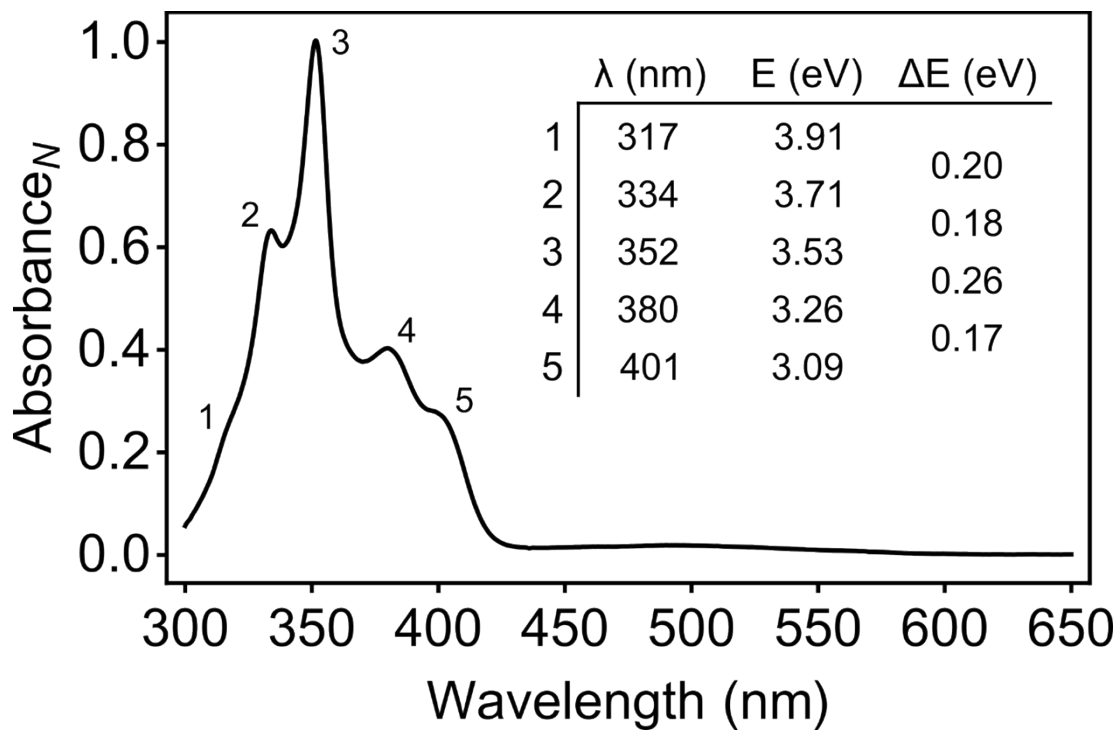


Figure S5. Normalized absorbance spectrum of *hex*-C6FE in CHCl₃, with labels for transitions.

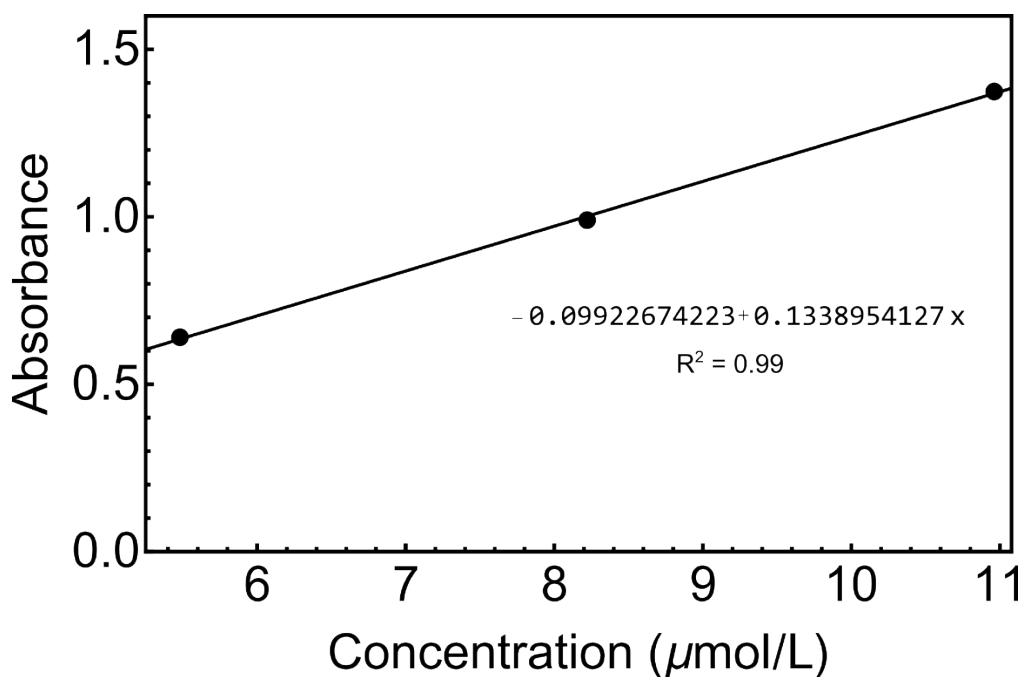


Figure S6. Beer's Law plot for *hex*-C6FE. Spectra collected in CHCl₃.

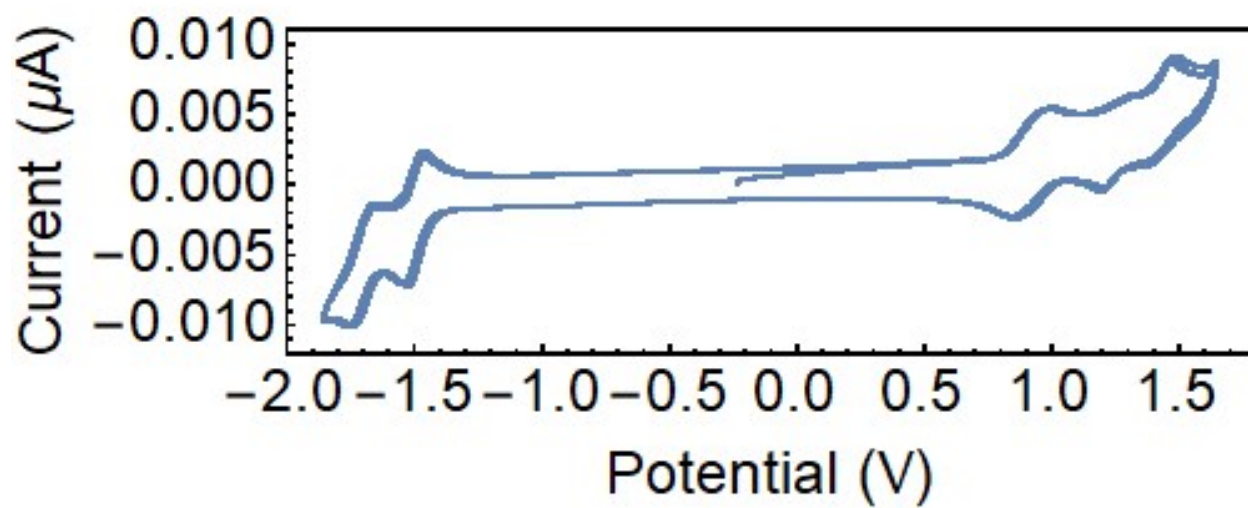


Figure S7. CV cycling experiment with *hex*-C6FE in CH₂Cl₂ with NBu₄PF₆ as the supporting electrolyte (0.1 M). Minimal change was observed in the voltammogram after multiple cycles.

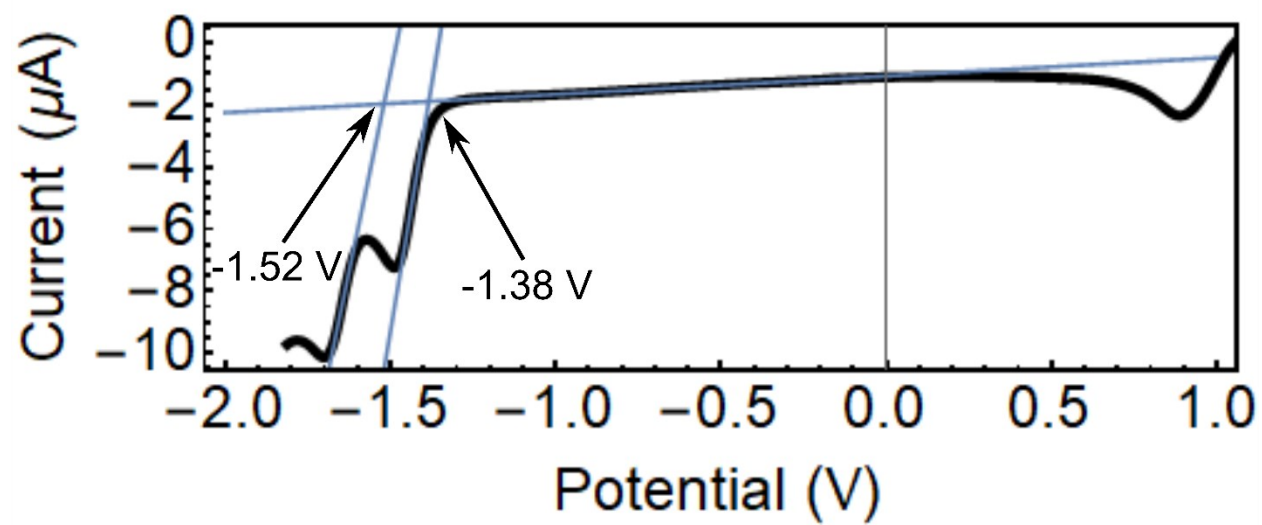
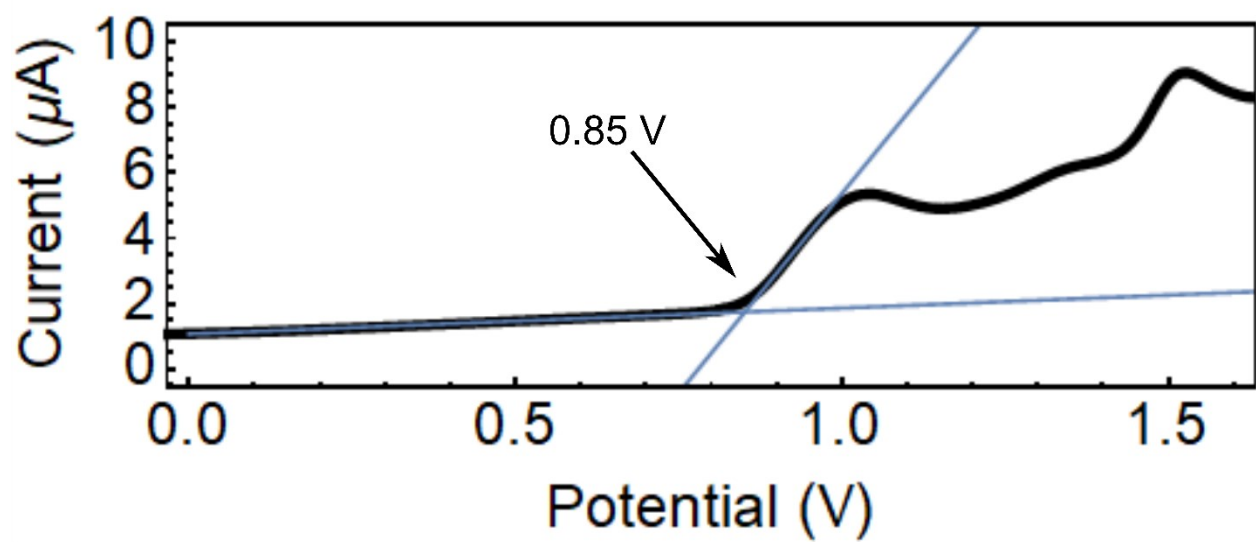


Figure S8. Determination of onset potentials in CV experiment.

NMR Spectra

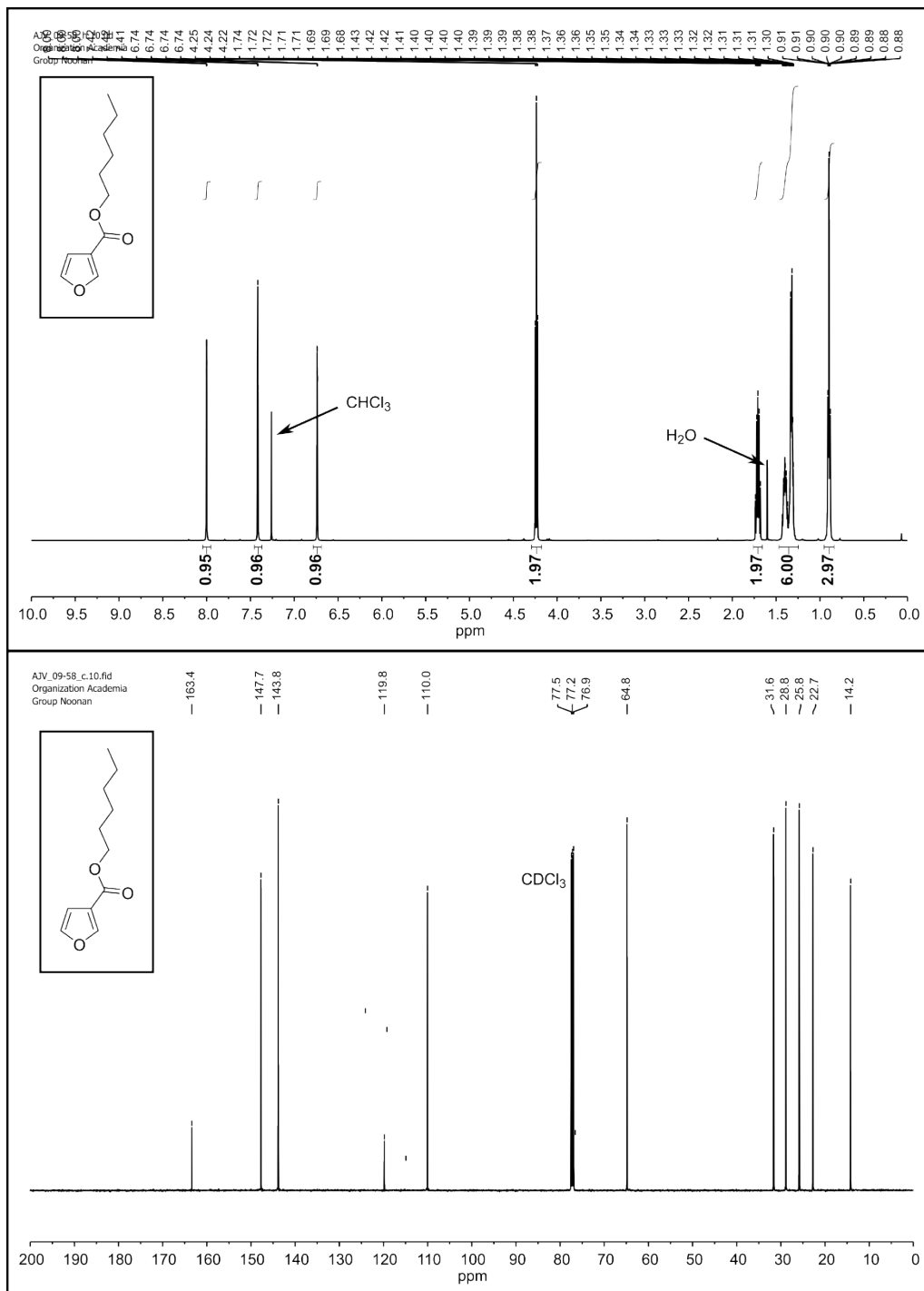


Figure S9. ¹H NMR spectrum (Top, 500 MHz, CDCl₃) and ¹³C NMR spectrum (Bottom, 126 MHz) of hexyl furan-3-carboxylate collected in CDCl₃.

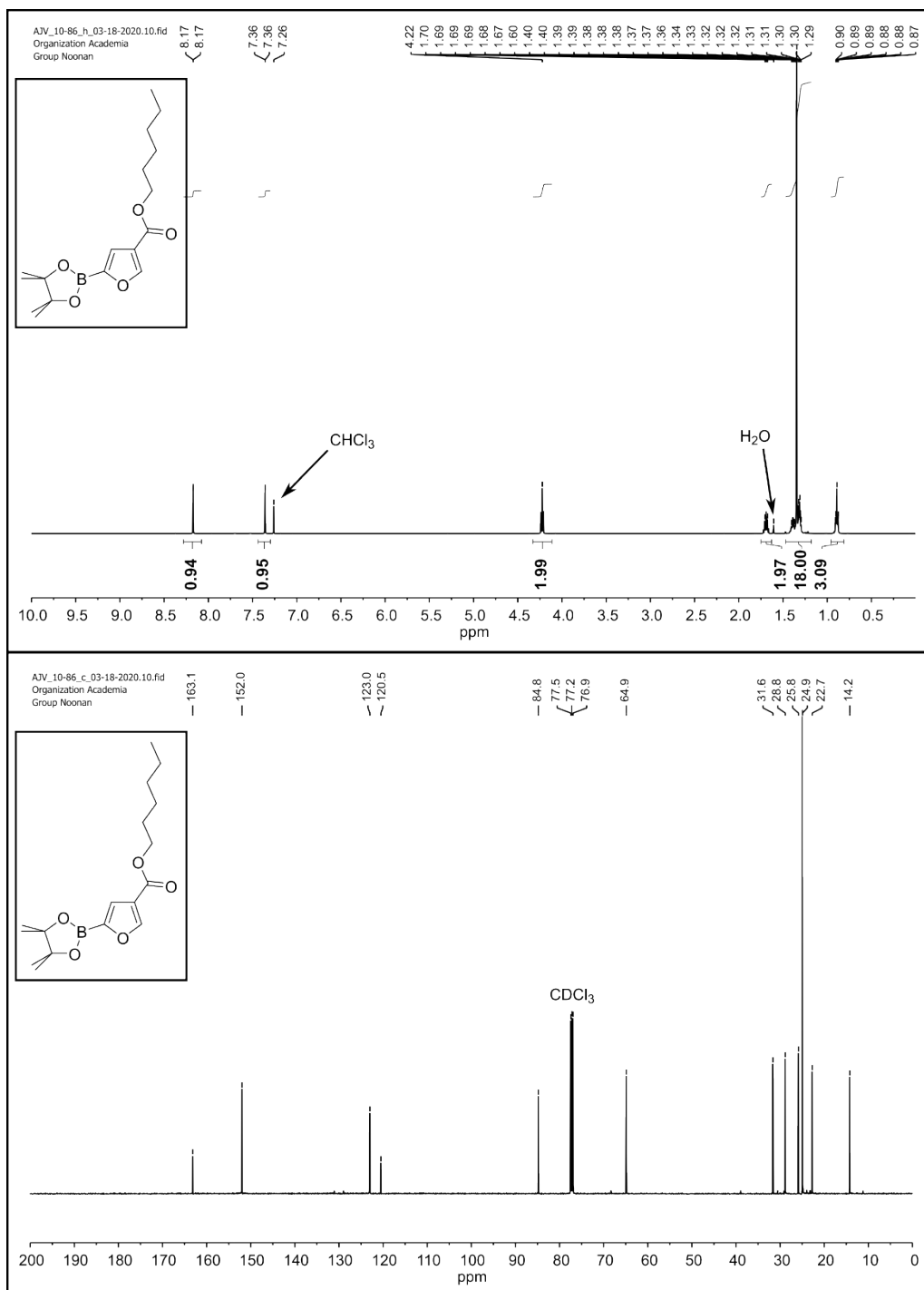


Figure S10a. ¹H NMR spectrum (Top, 500 MHz, CDCl₃) and ¹³C NMR spectrum (Bottom, 126 MHz) of hexyl 5-(4,4,5,5-tetramethyl-1,3,2-dioxaborolan-2-yl)furan-3-carboxylate collected in CDCl₃.

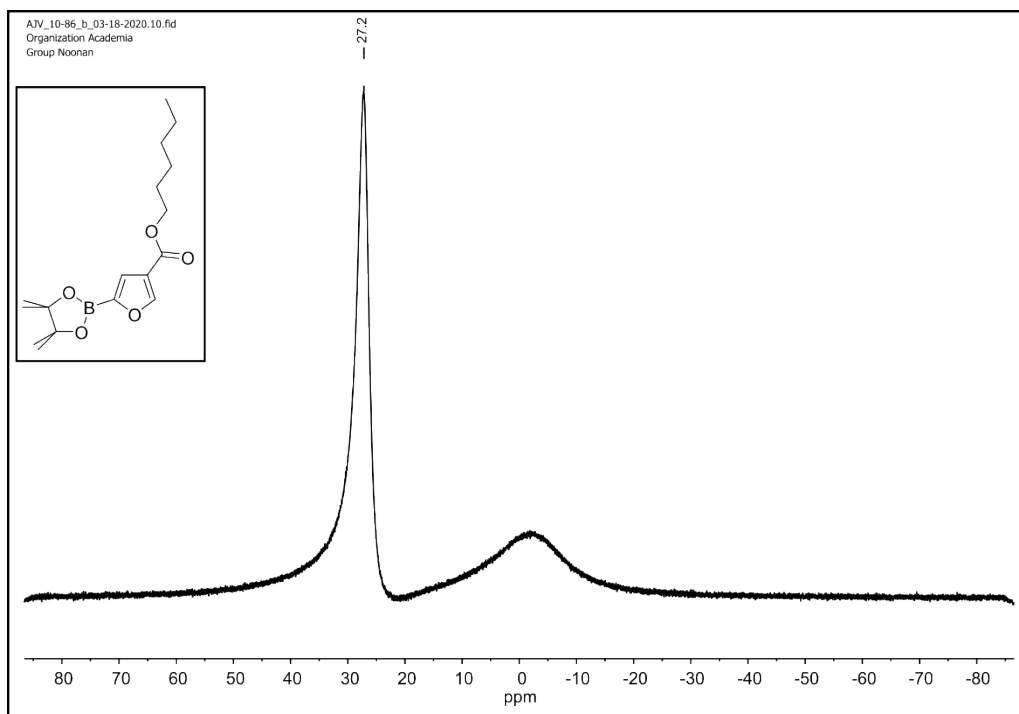


Figure S10b. ^{11}B NMR spectrum (160 MHz, CDCl_3) of hexyl 5-(4,4,5,5-tetramethyl-1,3,2-dioxaborolan-2-yl)furan-3-carboxylate collected in CDCl_3 .

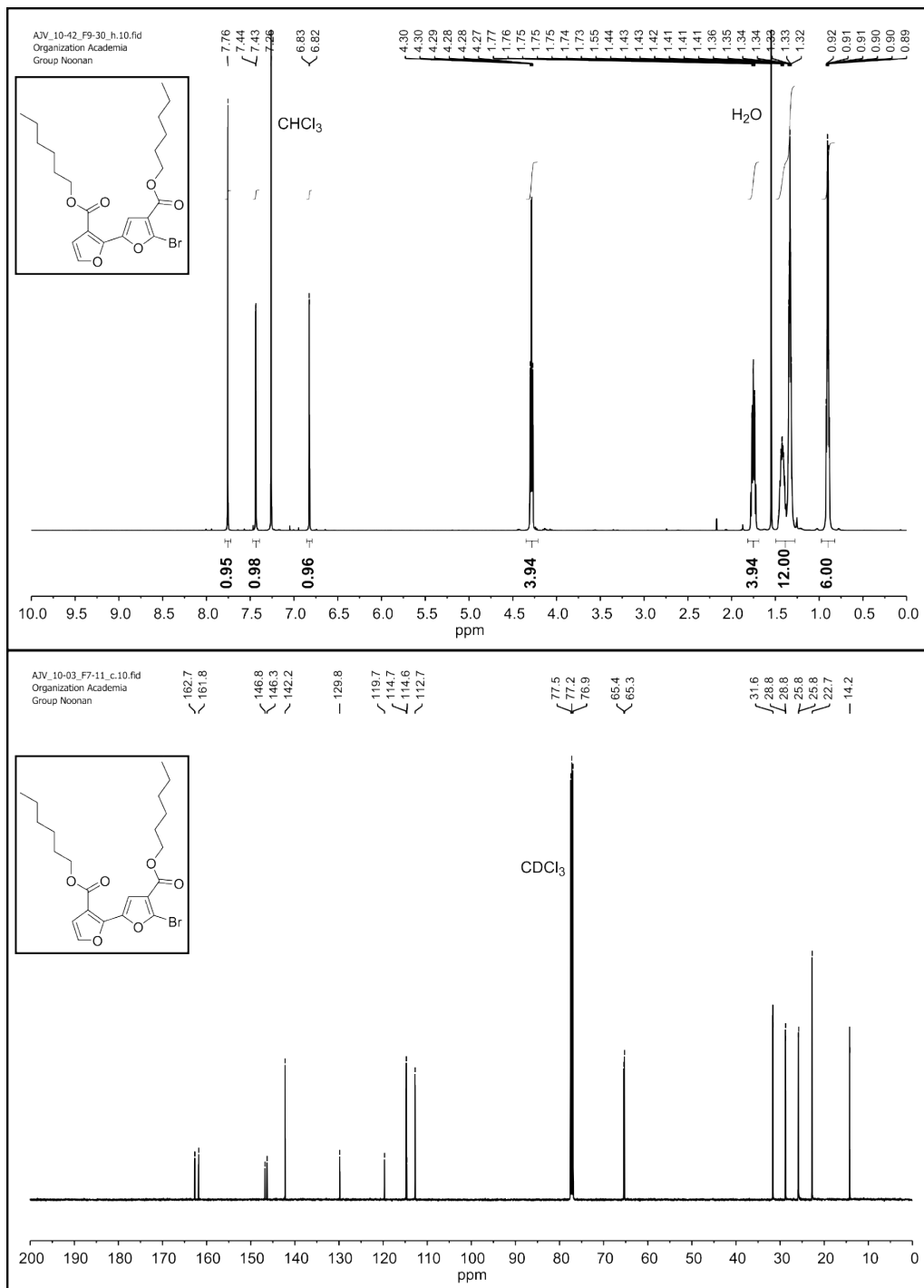


Figure S12. ¹H NMR spectrum (Top, 500 MHz, CDCl₃) and ¹³C NMR spectrum (Bottom, 126 MHz) of dihexyl 5'-bromo-[2,2'-bifuran]-3,4'-dicarboxylate collected in CDCl₃.

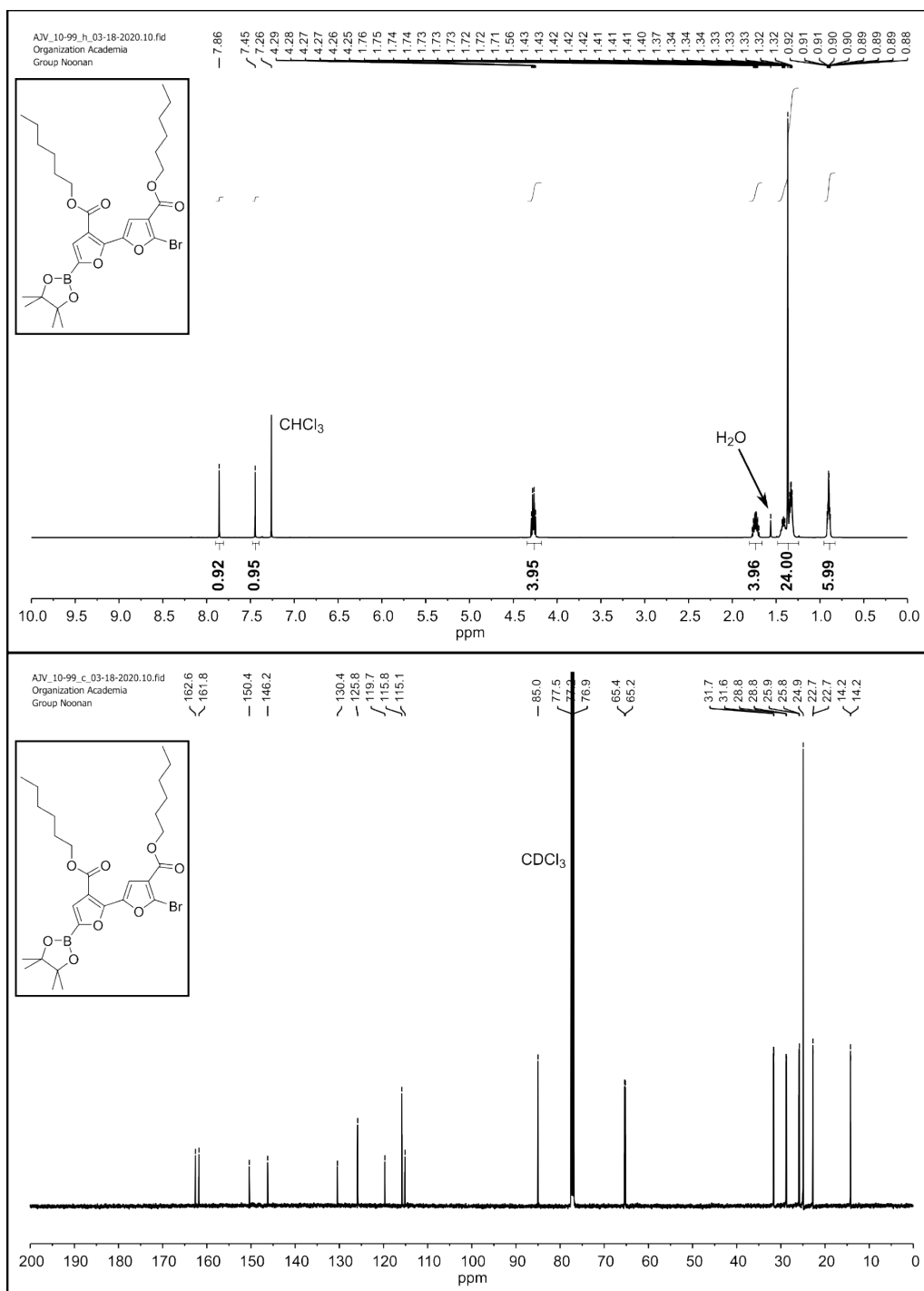


Figure S13a. ¹H NMR spectrum (Top, 500 MHz, CDCl₃) and ¹³C NMR spectrum (Bottom, 126 MHz) of dihexyl 5'-bromo-5-(4,4,5,5-tetramethyl-1,3,2-dioxaborolan-2-yl)-[2,2'-bifuran]-3,4'-dicarboxylate collected in CDCl₃.

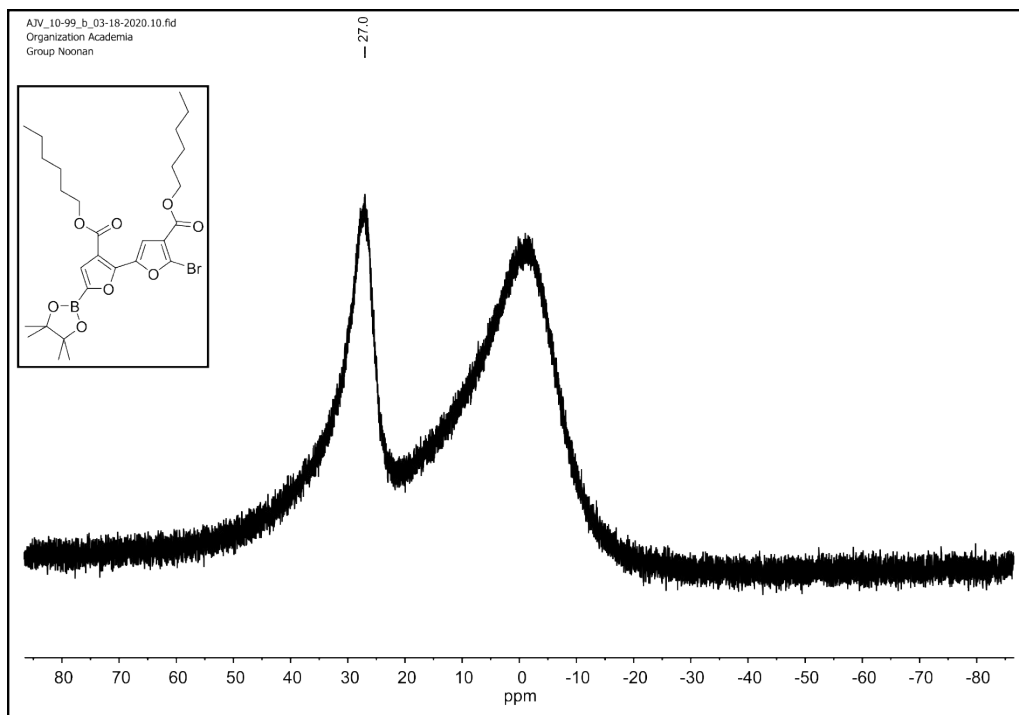


Figure S13b. ^{11}B NMR spectrum (160 MHz, CDCl_3) of dihexyl 5'-bromo-5-(4,4,5,5-tetramethyl-1,3,2-dioxaborolan-2-yl)-[2,2'-bifuran]-3,4'-dicarboxylate collected in CDCl_3 .

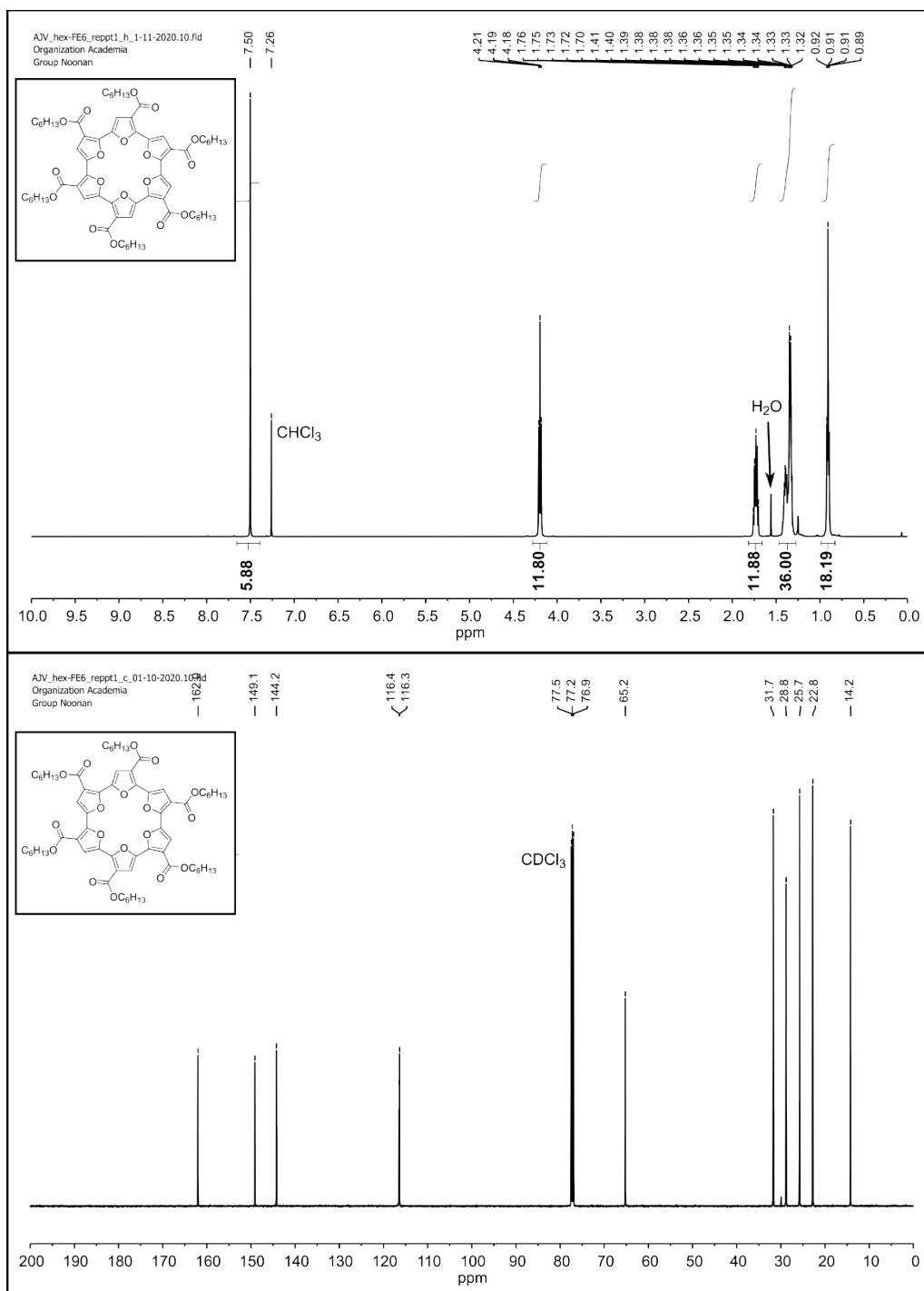


Figure S14. ¹H NMR spectrum (Top, 500 MHz, CDCl₃) and ¹³C NMR spectrum (Bottom, 126 MHz) of hexyl-ester macrocycle (*hex-C6FE*) collected in CDCl₃.

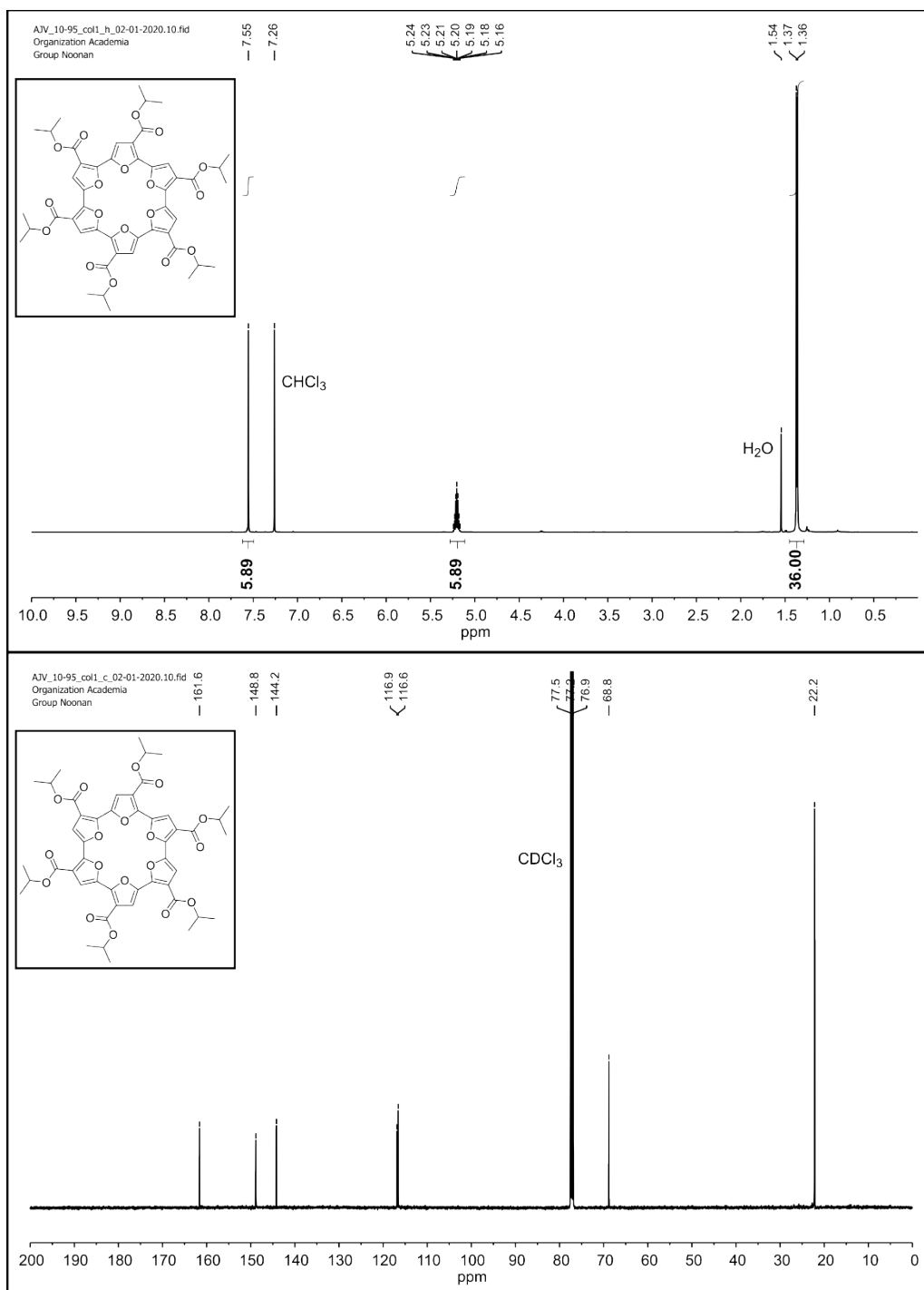


Figure S15. ¹H NMR spectrum (Top, 500 MHz, CDCl₃) and ¹³C NMR spectrum (Bottom, 126 MHz) of isopropyl-ester macrocycle (*ipr*-C6FE) collected in CDCl₃.

HRMS

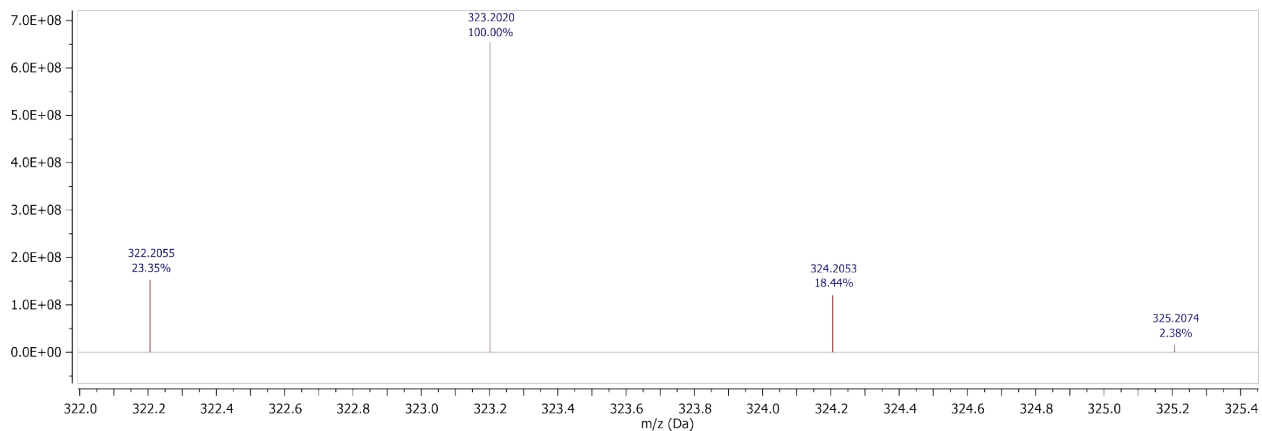


Figure S16. DART-MS of hexyl 5-(4,4,5,5-tetramethyl-1,3,2-dioxaborolan-2-yl)furan-3-carboxylate.

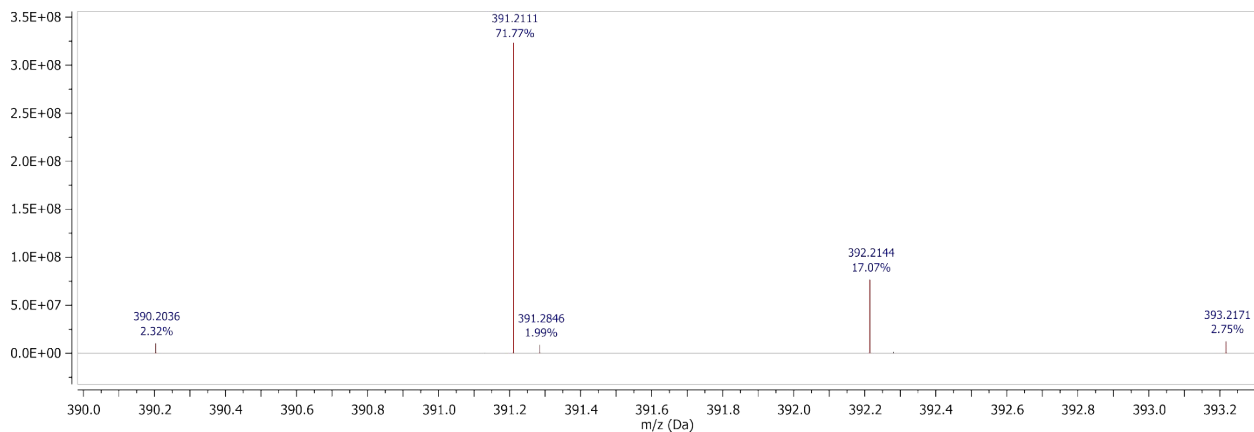


Figure S17. DART-MS of dihexyl [2,2'-bifuran]-3,4'-dicarboxylate.

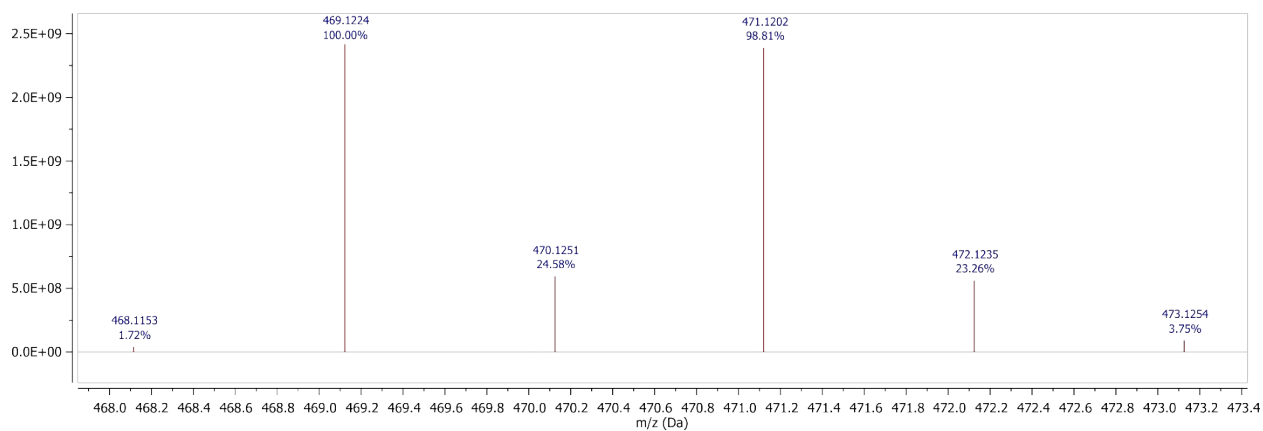


Figure S18. DART-MS of dihexyl 5'-bromo-[2,2'-bifuran]-3,4'-dicarboxylate.

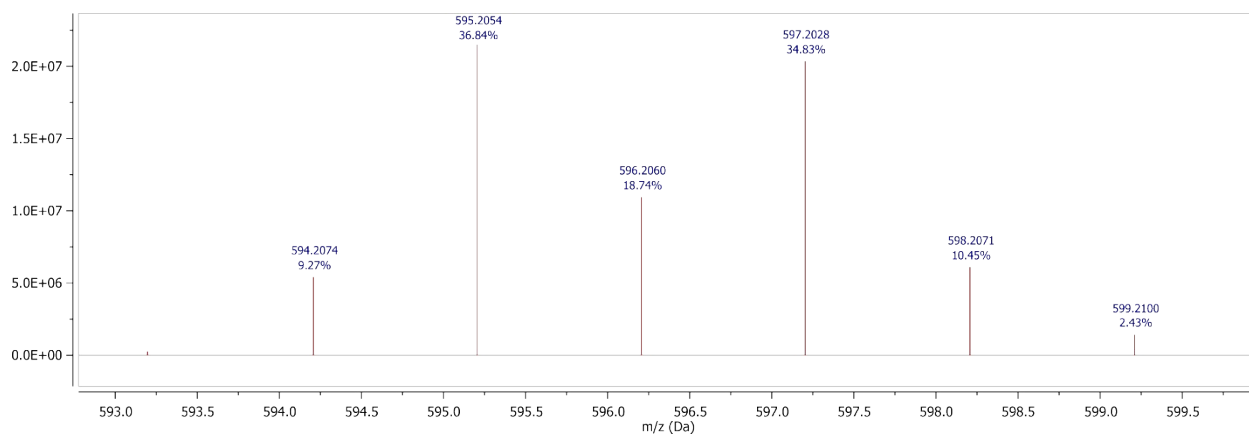


Figure 19. DART-MS of dihexyl 5'-bromo-5-(4,4,5,5-tetramethyl-1,3,2-dioxaborolan-2-yl)-[2,2'-bifuran]-3,4'-dicarboxylate.

Frontier Orbitals and Doubly Charged States.

Table S1. HOMO, LUMO and total energy comparisons for the open and cyclic variants of sexifurans using B3LYP 6-31G(d,p) IEFPCM(CH₂Cl₂).

	HOMO (eV)	LUMO (eV)
6F	-4.70	-1.72
6FE	-5.26	-2.34
C6F	-4.45	-1.91
C6FE	-5.13	-2.61

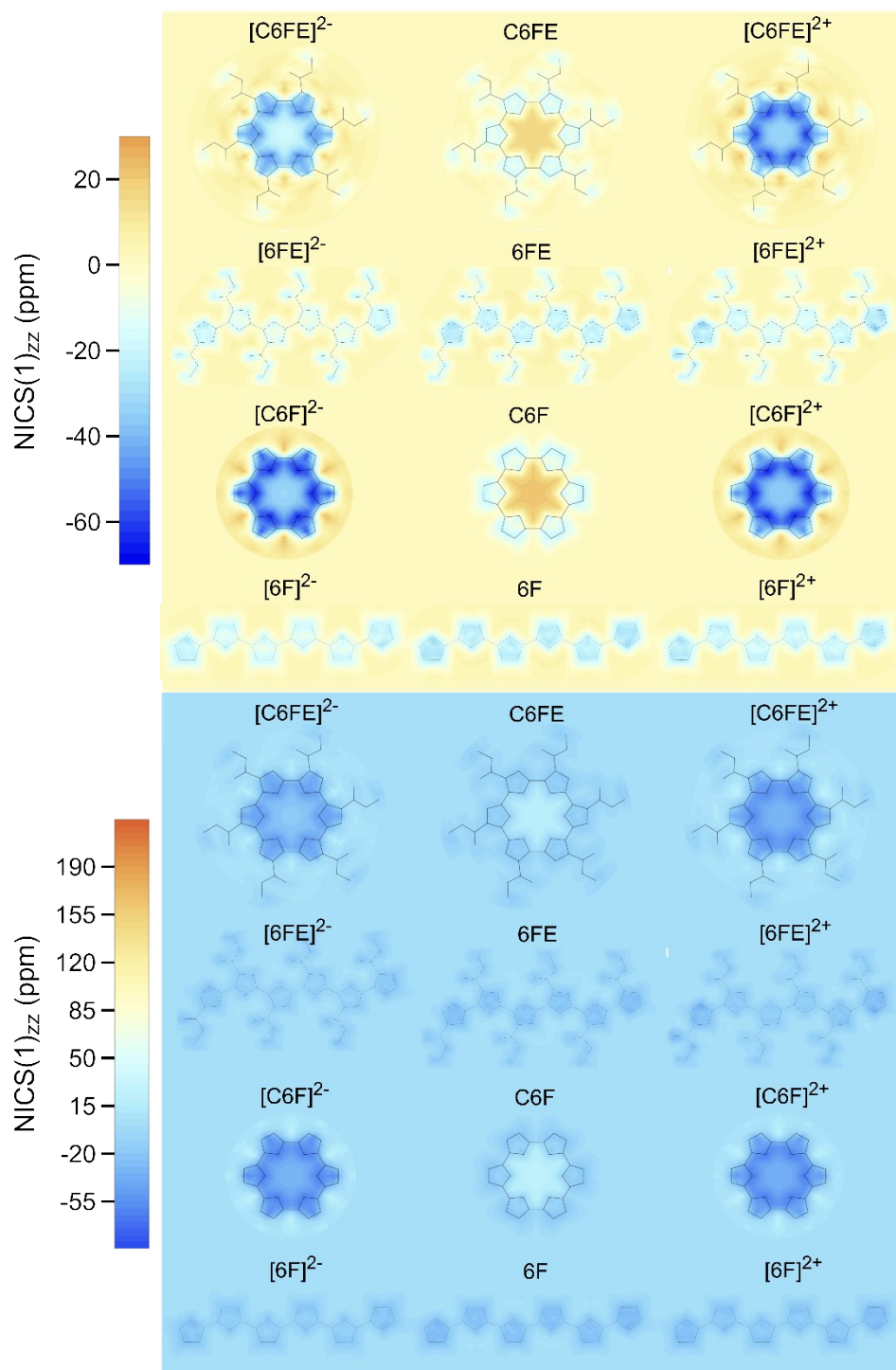


Figure S20. NICS (B3LYP/6-31G(d,p) IEFPCM/CH₂Cl₂) plots of optimized singlet state structures for bare and methyl-ester substituted sexifuran oligomers (**C6FE**, **6FE**, **C6F**, **6F**), plotted with two different ranges. For each structure, the neutral, dianionic, and dicationic species are shown.

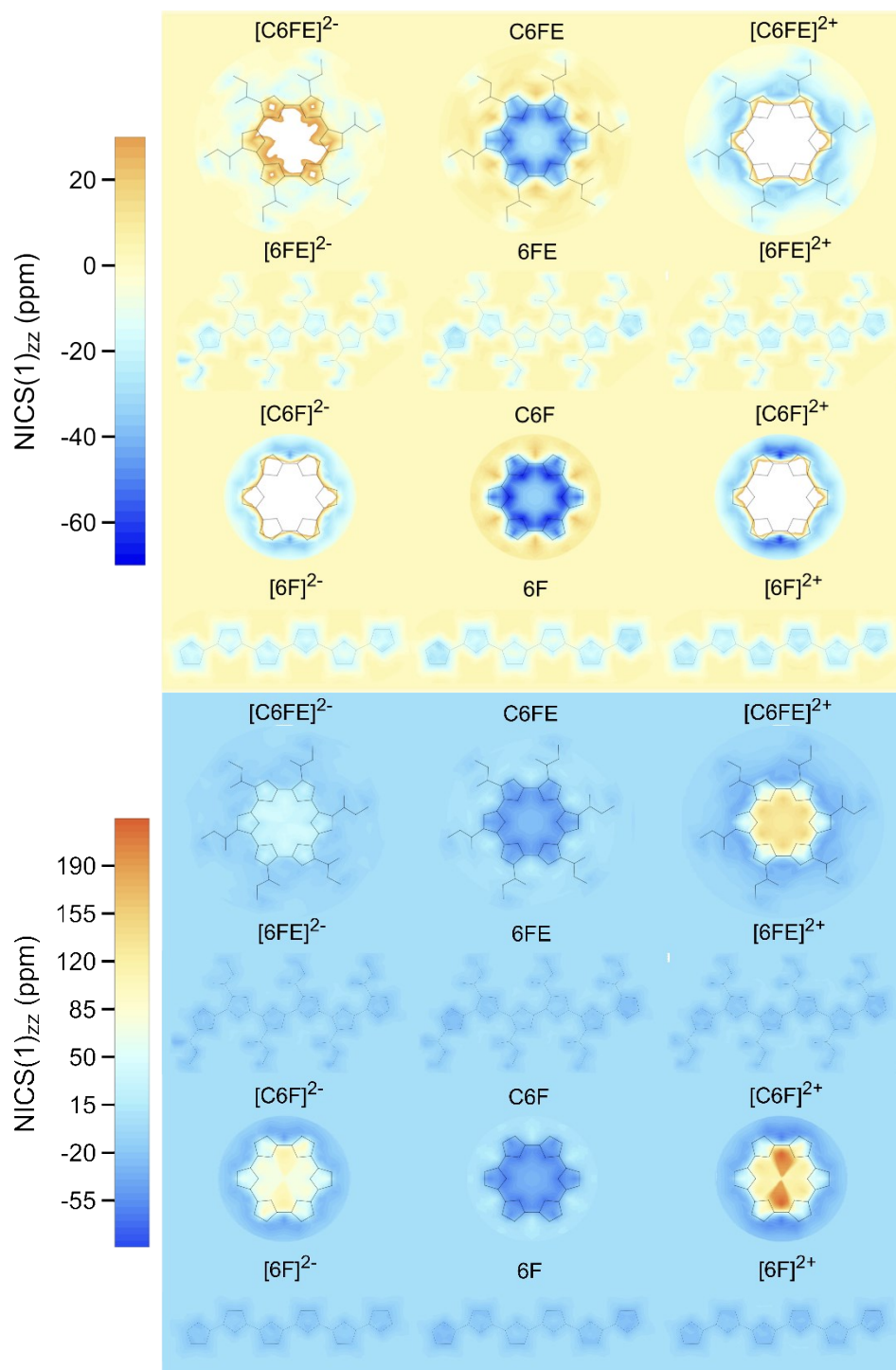


Figure S21. NICS (B3LYP/6-31G(d,p) IEFPCM/CH₂Cl₂) plots of optimized triplet state structures for bare and methyl-ester substituted sexifuran oligomers (**C6FE**, **6FE**, **C6F**, **6F**), plotted with two different ranges. For each structure, the neutral, dianionic, and dicationic species are shown.

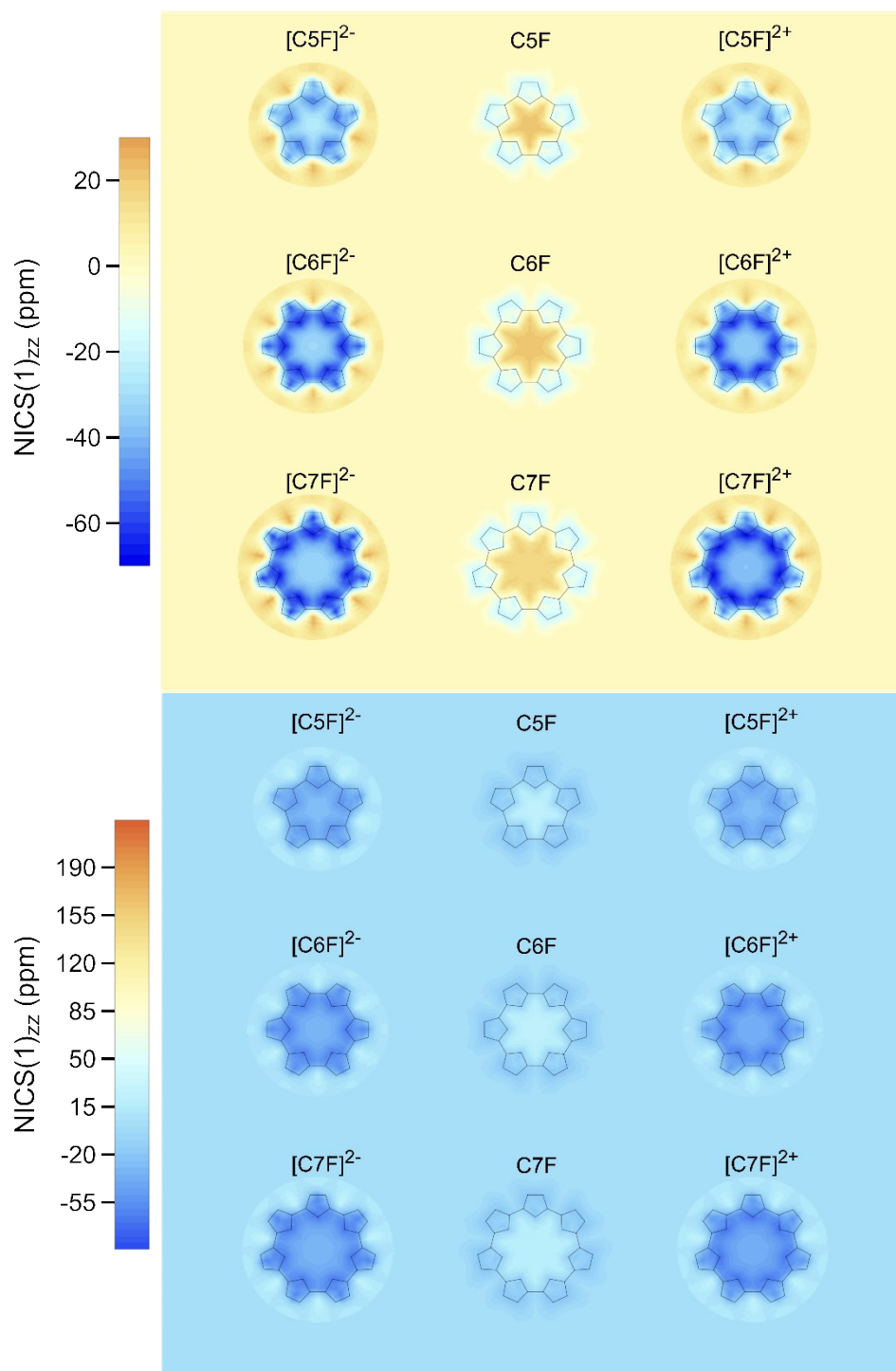


Figure S22. NICS (B3LYP/6-31G(d,p) IEFPCM/CH₂Cl₂) plots of optimized singlet state structures for bare macrocyclic oligofurans composed of 5-7 repeat units (**C5F**, **C6F**, **C7F**), plotted with two different ranges. For each structure, the neutral, dianionic, and dicationic species are shown.

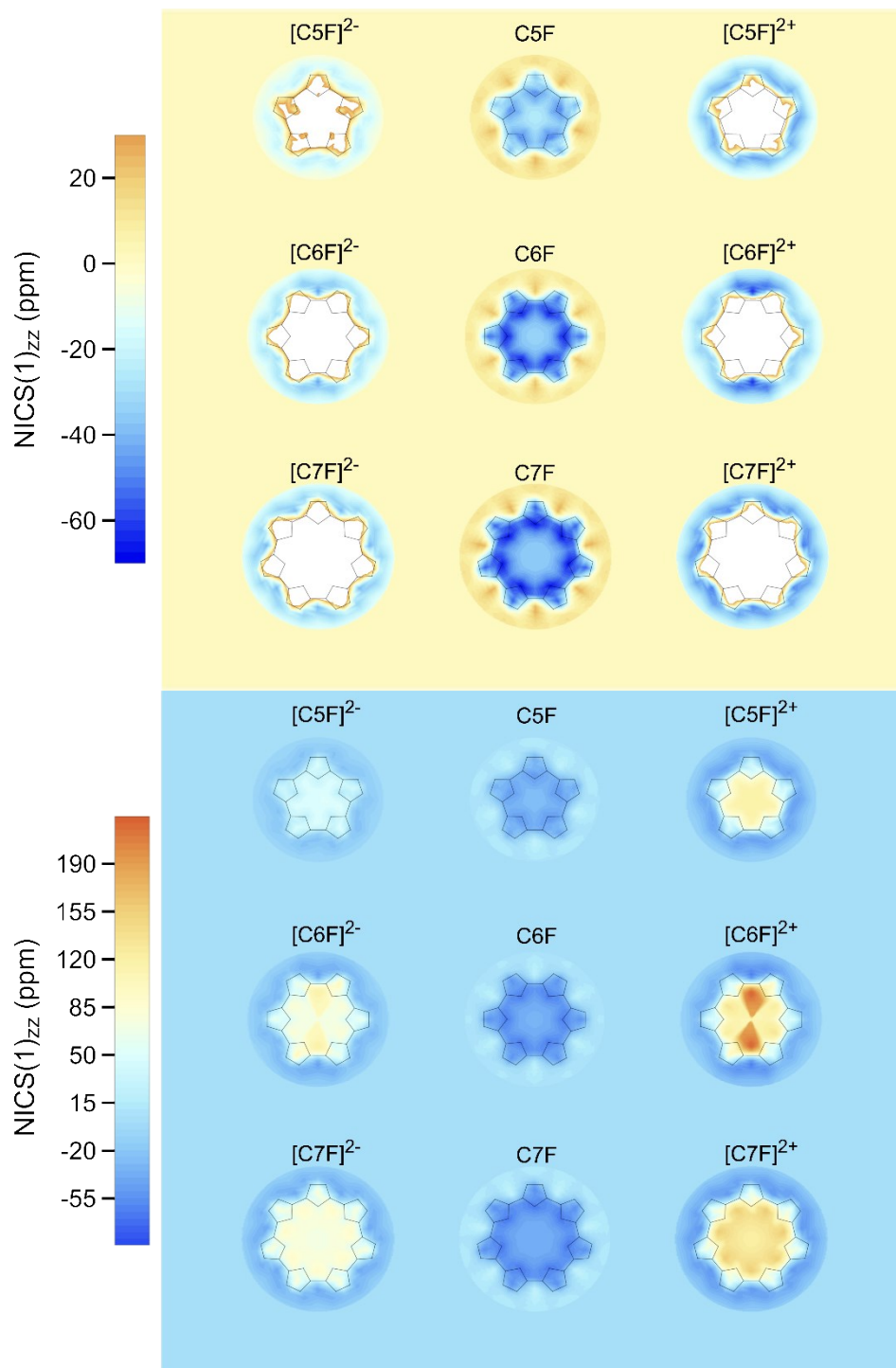


Figure S23. NICS (B3LYP/6-31G(d,p) IEFPCM/CH₂Cl₂) plots of optimized triplet state structures for bare macrocyclic oligofurans composed of 5-7 repeat units (**C₅F**, **C₆F**, **C₇F**), plotted with two different ranges. For each structure, the neutral, dianionic, and dicationic species are shown.

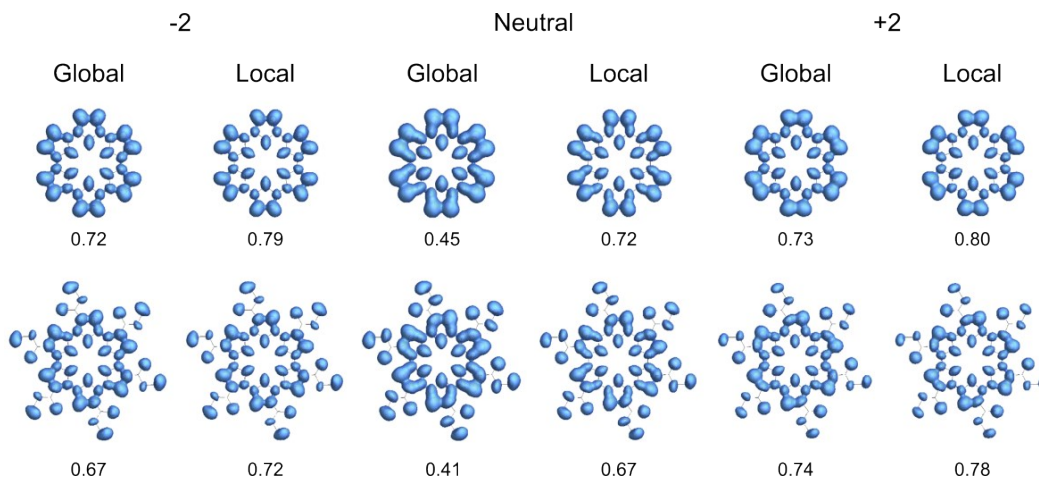


Figure S24. Electron localization function (ELF) plots of **C6F** (top) and methyl-ester substituted **C6FE** (bottom).

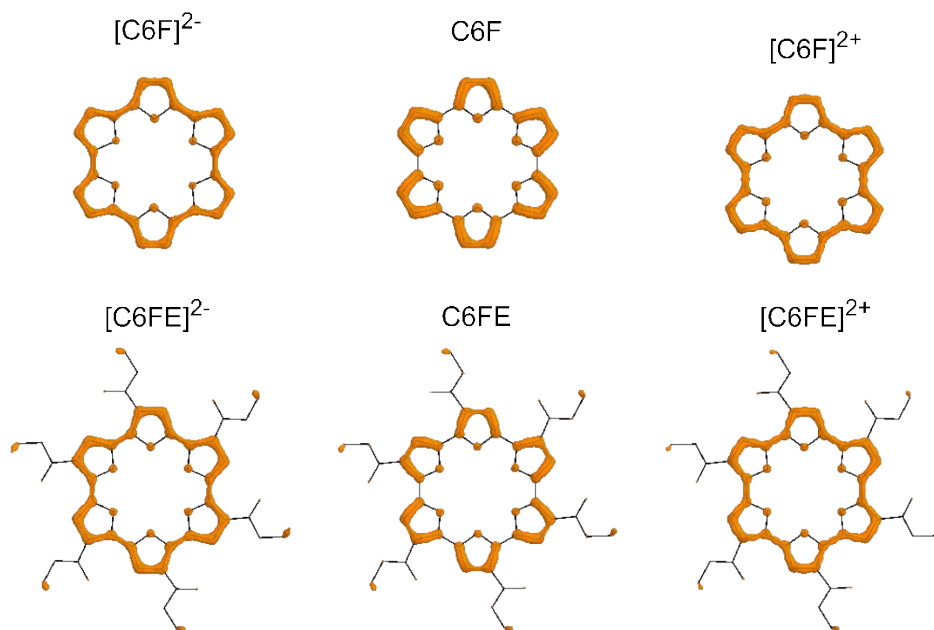


Figure S25. Localized-orbital locator (LOL) plots of **C6F** and **C6FE**.

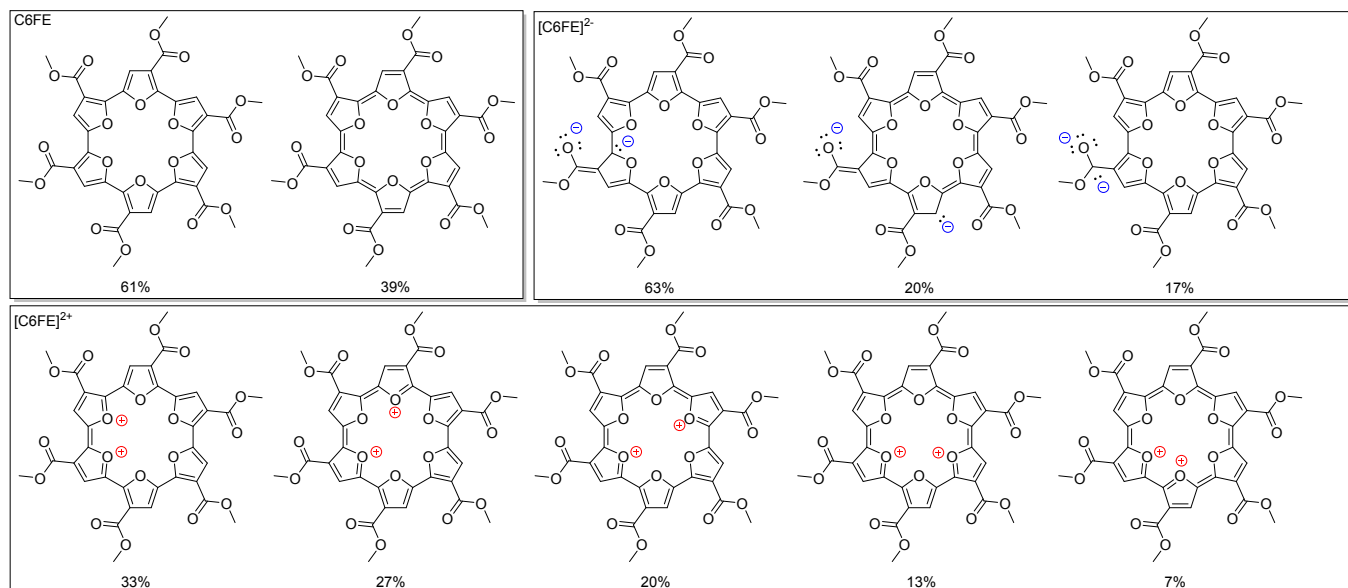


Figure S26. Resonance structures predicted by Natural Resonance Theory (NRT) for [C6FE]²⁻ (left), C6FE (middle), and [C6FE]²⁺ (right). The percent value below each structure corresponds to contribution to the overall form.

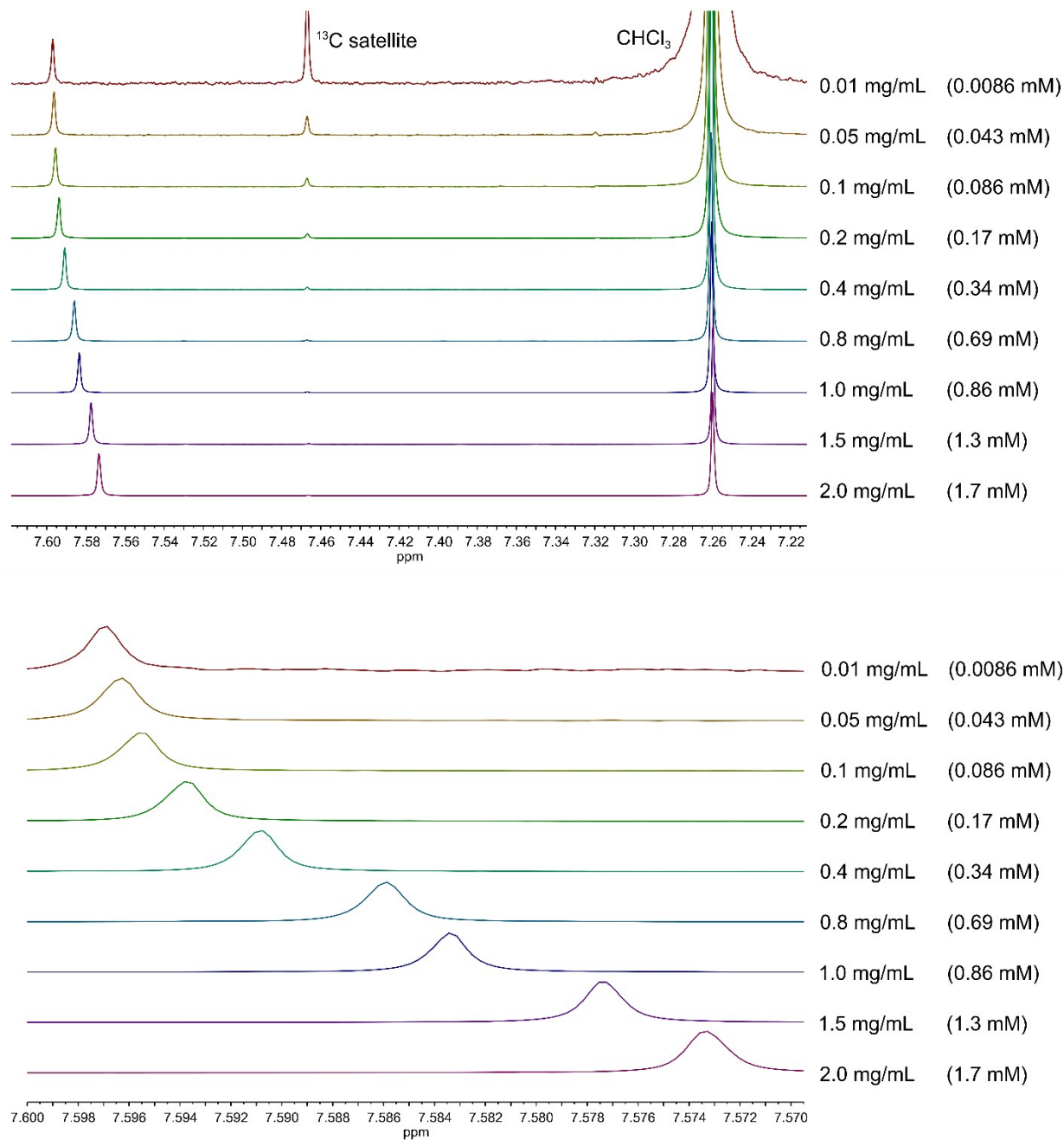


Figure S27. ^1H NMR chemical shift of aromatic signal for *hex*-C₆FE in CDCl_3 at 295 K at varying concentrations.

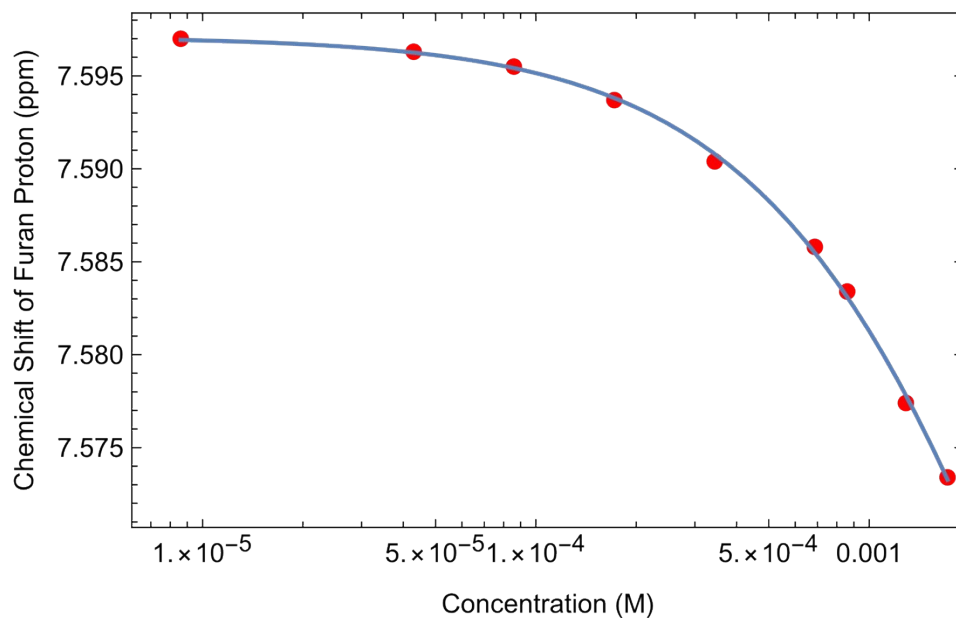


Figure S28. Semilogarithmic plot of ^1H NMR chemical shift of aromatic signal for *hex*-C6FE in CDCl_3 at concentrations specified in Figure S27 (red dots), fitted to monomer-dimer model equation (blue).

Monomer-Dimer Model.¹¹⁻¹³ The equation below predicts the chemical shift changes as a function of concentration assuming an equilibrium between monomeric and dimeric species.

$$\delta = (\delta_d - \delta_m) \left(1 + \frac{1 - \sqrt{1 + 8K_a C}}{4K_a C} \right) + \delta_m$$

Where:

δ = observed chemical shift

δ_m = chemical shift of monomer

δ_d = chemical shift of dimer

K_a = association constant

C = total concentration

References

1. A. J. Varni, A. Fortney, M. A. Baker, J. C. Worch, Y. Qiu, D. Yaron, S. Bernhard, K. J. T. Noonan and T. Kowalewski, Photostable Helical Polyfurans, *J. Am. Chem. Soc.*, 2019, **141**, 8858-8867.
2. N. G. Connelly and W. E. Geiger, Chemical Redox Agents for Organometallic Chemistry, *Chem. Rev.*, 1996, **96**, 877-910.
3. Gaussian 09, Revision A.02, M. J. Frisch, G. W. Trucks, H. B. Schlegel, G. E. Scuseria, M. A. Robb, J. R. Cheeseman, G. Scalmani, V. Barone, G. A. Petersson, H. Nakatsuji, X. Li, M. Caricato, A. Marenich, J. Bloino, B. G. Janesko, R. Gomperts, B. Mennucci, H. P. Hratchian, J. V. Ortiz, A. F. Izmaylov, J. L. Sonnenberg, D. Williams-Young, F. Ding, F. Lipparini, F. Egidi, J. Goings, B. Peng, A. Petrone, T. Henderson, D. Ranasinghe, V. G. Zakrzewski, J. Gao, N. Rega, G. Zheng, W. Liang, M. Hada, M. Ehara, K. Toyota, R. Fukuda, J. Hasegawa, M. Ishida, T. Nakajima, Y. Honda, O. Kitao, H. Nakai, T. Vreven, K. Throssell, J. A. Montgomery, Jr., J. E. Peralta, F. Ogliaro, M. Bearpark, J. J. Heyd, E. Brothers, K. N. Kudin, V. N. Staroverov, T. Keith, R. Kobayashi, J. Normand, K. Raghavachari, A. Rendell, J. C. Burant, S. S. Iyengar, J. Tomasi, M. Cossi, J. M. Millam, M. Klene, C. Adamo, R. Cammi, J. W. Ochterski, R. L. Martin, K. Morokuma, O. Farkas, J. B. Foresman, and D. J. Fox, Gaussian, Inc., Wallingford CT, 2016.
4. E.D. Glendening, J. K. Badenhoop, A. E. Reed, J. E. Carpenter, J. A. Bohmann, C. M. Morales, P. Karafiloglou, C. R. Landis, and F. Weinhold. NBO 7.0; Theoretical Chemistry Institute, University of Wisconsin: Madison, WI, 2018.
5. H. L. Schmider and A. D. Becke, Two functions of the density matrix and their relation to the chemical bond, *J. Chem. Phys.*, 2002, **116**, 3184-3193.
6. H. L. Schmider and A. D. Becke, Chemical content of the kinetic energy density, *J. Mol. Struct.: THEOCHEM*, 2000, **527**, 51-61.
7. A. D. Becke and K. E. Edgecombe, A simple measure of electron localization in atomic and molecular systems, *J. Chem. Phys.*, 1990, **92**, 5397-5403.
8. T. Lu and F. Chen, Multiwfn: A multifunctional wavefunction analyzer, *J. Comput. Chem.*, 2012, **33**, 580-592.
9. T. Lu and F.-W. Chen, Meaning and Functional Form of the Electron Localization Function, *Acta Phys. -Chim. Sin.*, 2011, **27**, 2786-2792.
10. O. Dishi and O. Gidron, Macrocyclic Oligofurans: A Computational Study, *J. Org. Chem.*, 2018, **83**, 3119-3125.
11. R. B. Martin, Comparisons of Indefinite Self-Association Models, *Chem. Rev.*, 1996, **96**, 3043-3064.
12. M. Chu, A. N. Scioneaux and C. S. Hartley, Solution-Phase Dimerization of an Oblong Shape-Persistent Macrocyclic, *J. Org. Chem.*, 2014, **79**, 9009-9017.
13. P. T. Lynett and K. E. Maly, Synthesis of Substituted Trinaphthylenes via Aryne Cyclotrimerization, *Org. Lett.*, 2009, **11**, 3726-3729.